Review article

Zeolite imidazolate framework-8 in bone regeneration: A systematic review

Hao Tang [a], Yameng Yu [a], Xinxin Zhan [a], Yuan Chai [a], Yufeng Zheng [b], Yunsong Liu [c,*], Dandan Xia [a,*], Hong Lin [a,*]

[a] Department of Dental Materials, Peking University School and Hospital of Stomatology & National Center of Stomatology & National Clinical Research Center for Oral Diseases & National Engineering Research Center of Oral Biomaterials and Digital Medical Devices & Beijing Key Laboratory of Digital Stomatology & Research Center of Engineering and Technology for Computerized Dentistry Ministry of Health & NMPA Key Laboratory for Dental Materials, Beijing 100081, China
[b] School of Materials Science and Engineering, Peking University, Beijing 100871, China
[c] Department of Prosthodontics, Peking University School and Hospital of Stomatology & National Center of Stomatology & National Clinical Research Center for Oral Diseases & National Engineering Research Center of Oral Biomaterials and Digital Medical Devices & Beijing Key Laboratory of Digital Stomatology & Research Center of Engineering and Technology for Computerized Dentistry Ministry of Health & NMPA Key Laboratory for Dental Materials, Beijing 100081, China

ARTICLE INFO

ABSTRACT

Zeolite imidazolate framework-8 (ZIF-8) is a biomaterial that has been increasingly studied in recent years. It has several applications such as bone regeneration, promotion of angiogenesis, drug loading, and antibacterial activity, and exerts multiple effects to deal with various problems in the process of bone regeneration. This systematic review aims to provide an overview of the applications and effectiveness of ZIF-8 in bone regeneration. A search of papers published in the PubMed, Web of Science, Embase, and Cochrane Library databases revealed 532 relevant studies. Title, abstract, and full-text screening resulted in 39 papers being included in the review, including 39 in vitro and 22 animal studies. Appropriate concentrations of nano ZIF-8 can promote cell proliferation and osteogenic differentiation by releasing Zn^{2+} and entering the cell, whereas high doses of ZIF-8 are cytotoxic and inhibit osteogenic differentiation. In addition, five studies confirmed that ZIF-8 exhibits good vasogenic activity. In all in vivo experiments, nano ZIF-8 promoted bone formation. These results indicate that, at appropriate concentrations, materials containing ZIF-8 promote bone regeneration more than materials without ZIF-8, and with characteristics such as promoting angiogenesis, drug loading, and antibacterial activity, it is expected to show promising applications in the field of bone regeneration.

Statement of significance: This manuscript reviewed the use of ZIF-8 in bone regeneration, clarified the biocompatibility and effectiveness in promoting bone regeneration of ZIF-8 materials, and discussed the possible mechanisms and factors affecting its promotion of bone regeneration. Overall, this study provides a better understanding of the latest advances in the field of bone regeneration of ZIF-8, serves as a design guide, and contributes to the design of future experimental studies.

1. Introduction

Bone is a highly dynamic structure with self-regenerative and self-healing abilities [1]; these processes involve a complex and dynamic balance between old bone breakdown and new bone regeneration [2], which is essential for the bone to regain its regular functions such as bearing, activity, protection, hematopoiesis, and endocrine homeostasis [3]. The regenerative ability of bone has long been recognized; however, beyond a critical defect size, the spontaneous repair and regeneration of bone is limited [4]. The main reasons for the failure of regeneration in severe bone defects are low intrinsic regenerative capacity, excessively

large bone volume requirement to fill the defect, and the bone tissue being affected by specific conditions such as osteonecrosis, tumors, or congenital abnormalities [5].

Bone grafts and alternatives from multiple sources have been used to address these critical size defects [6]. Depending on the source of the implant, they can be divided into autografts, allogeneic grafts, and bone graft substitutes [7]. Of these, autologous bone grafts have the best osteogenic potential and are generally considered the gold standard; however, the limited quantity of autografts for harvest and donor-site morbidity limit their use [7]. Thus, allogeneic grafts and bone graft substitutes have been introduced, whose advantages include their

---

* Corresponding authors.
E-mail addresses: liuyunsong@hsc.pku.edu.cn (Y. Liu), dandanxia@pku.edu.cn (D. Xia), hong196lin@bjmu.edu.cn (H. Lin).

availability and lack of injury to the donor site [8]. Bone substitutes including tricalcium phosphate (TCP), hydroxyapatite (HAp), calcium sulfate, demineralized bone matrix, and bone morphogenetic protein (BMP) have been extensively studied [9]. There are many requirements for materials for bone tissue regeneration [10,11]; they should not only have bone-stimulating effects but also exhibit antibacterial, anti-inflammatory, and anticancer effects [12,13]. However, so far, no ideal bone substitutes have been found.

Metal-organic frameworks (MOFs), which originated in the 1990s and have developed rapidly in the last couple of years, are new multi-functional materials composed of central metal ions and organic ligands and exhibiting unique characteristics such as porous structure, ultrahigh surface area, and structural diversity [14]. Pertinent examples include MOF-74, MIL-100(Fe), and ZIFs [15]. Because of these features, MOFs have attracted considerable attention in recent years. In medicine, MOFs find applications in biomedical imaging [16], tumor treatment [17], and targeted drug delivery [18], among others. Given their special properties, investigators have started focusing on the production of MOF-based composite bone materials to overcome the limitations and shortcomings of bone repair materials currently in use.

Zeolitic imidazolate framework-8 (ZIF-8) is a subclass of MOF formed via the coordination of zinc ions (Zn^{2+}) with 2-methylimidazole (MeIm) [19]. It stands out for its negligible cytotoxicity, excellent chemical and thermal stability, and pH sensitivity, making it a promising candidate for bone regeneration [20]. The biocompatibility of ZIF-8 is reflected in the harmlessness of its constituent components; as a necessary trace element for the human body, Zn^{2+} is an endogenous metal cation with low toxicity, and the imidazole group is also found in the amino acid histamine [21,22]. Zn^{2+} produced by ZIF-8 degradation not only triggers good bone stimulation at suitable concentrations [23] but also can exert good antibacterial function [24]. ZIF-8 also has a large specific surface area and high pore volume, indicating that the material has a high drug load. The uniform pore size and pore distribution also ensure an even distribution of drugs and prevent their sudden release. Both these characteristics indicate that synthetic ZIF-8 is an excellent drug carrier [25] which can perform multiple functions by loading various types of drugs to tackle a variety of problems observed in the process of bone defect repair.

The objective of this review is to discuss the effectiveness of ZIF-8 in promoting osteogenesis in vitro and in vivo when used alone or in combination with other biological materials. Simultaneously, the relevant factors affecting the biocompatibility and osteogenic ability of ZIF-8, including its concentration, size, and modification mode, are analyzed, and the mechanism leading to the cytotoxicity of ZIF-8 and the related mechanism of promoting the osteogenic differentiation of cells are discussed with the aim of helping future research concerning ZIF-8 promoting osteogenesis.

2. Materials and methods

2.1. Protocol and search strategy

This systematic review was conducted in accordance with the Preferred Reporting Items for Systematic Reviews and Meta-Analyses (PRISMA) 2020 statement [26]. The focus question addressed was "Do the ZIF-8 materials promote osteogenesis?" conceived according to the population, intervention, control, and outcome (PICO) principles. Therefore, in this study, the population (P) is the group (cells or animals) that received treatment; intervention (I) corresponds to the treatment with ZIF-8 materials; comparison (C) is the control group or non-treated group; and outcome (O) denotes the parameters associated with osteogenesis, such as alkaline phosphatase (ALP) activity, gene expression, and production of mineralized extracellular matrix (MECM) or histological analyses and micro-computed tomography (micro-CT) for in

vitro and in vivo studies, respectively.

Some search strategies were developed based on these principles. In June 2023, literature searches were conducted on PubMed, Web of Science, Embase, and the Cochrane Library to identify publications. The following keywords were used: "Metal-Organic Frameworks" OR "Zeolites" OR "ZIF-8 metal-organic framework" AND "Osteogenesis" OR "Bone Regeneration." Details of the search strategies are provided in the Supplementary Document.

2.2. Inclusion/exclusion criteria

The inclusion criteria were as follows: (1) in vitro studies, (2) in vivo studies with animals, (3) ZIF-8 materials used alone or in combination with other biomaterials, (4) design of the experimental grouping reflecting the effect of ZIF-8 on osteogenesis, (5) evaluation of parameters related to bone regeneration, (6) research works only, and (7) published in English.

The exclusion criteria were as follows: (1) the biomaterial used is not or does not contain ZIF-8; (2) the experimental grouping design does not show the effect of ZIF-8 on osteogenesis (e.g., material A is used in combination with ZIF-8, and there is no separate material grouping to show the promoting or inhibiting effect of ZIF-8 on osteogenesis); (3) parameters regarding bone regeneration are not reported; (4) studies published in non-English; and (5) non-original studies, case reports, conference abstracts, editorials, letters, comments to editors, reviews, meta-analyses, book chapters, patents, etc.

2.3. Studies selection and data extraction

All articles obtained from the four databases were imported into the Reference Manager, and duplicates were removed. These records were screened primarily by title and abstract to identify studies that were within the scope of the review and met the inclusion criteria. After title and abstract screening, full-text articles were identified, screened, and reviewed. Studies that met any exclusion criteria during full-text screening were excluded. Details of the studies that met the criteria were extracted and recorded in data extraction tables.

3. Results

3.1. Study selection

This systematic review was conducted following the Preferred Reporting Items for Systematic Reviews and Meta-Analyses (PRISMA) 2020 statement [26]; a flowchart of the study selection process is shown in Fig. 1.

We identified 532 potential manuscripts in the initial search, retaining 363 records after removing duplicates. After screening the titles and abstracts, 311 records were excluded because they did not meet the inclusion criteria of "ZIF-8 materials used alone or in combination with other biomaterials," "research works only," and "published in English." After reading the remaining 52 papers in full, 39 were deemed eligible for review, of which 23 were in vitro only, and 29 were both in vitro and animal experiments. The studies were published between 2017 and June 2023, and showed a rapidly growing trend (Fig. 2). Of the excluded 13 papers, seven papers [17,27–32] were excluded because they did not report osteogenesis-related parameters, and six papers [33–38] were excluded because the experimental group design did not reflect the use of ZIF-8 in osteogenesis; three animal studies from the eligible 39 papers [35,39,40] were also excluded because the experimental group design did not reflect the effects of ZIF-8 on osteogenesis. The contents of the 39 papers included in the manuscript were systematically summarized, and 39 in vitro studies and 22 animal studies were included in the statistical analysis (Tables 1 and 2).
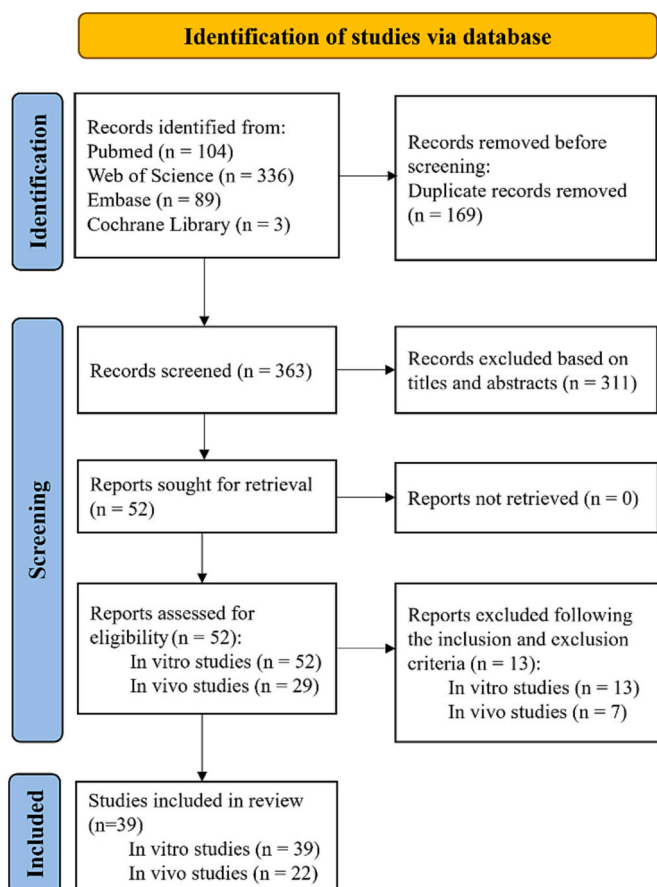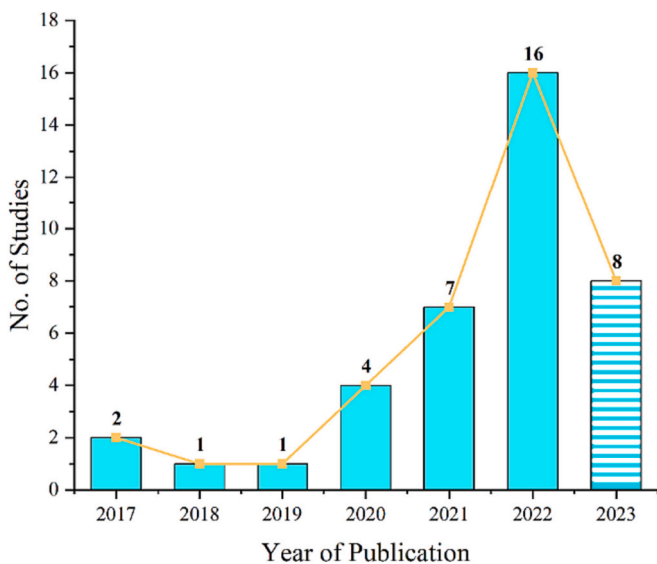
Fig. 1. PRISMA flow diagram.

Fig. 2. Number of published studies included in the systematic review sorted by the year of publication.

3.2. Material characteristics

ZIF-8 particles are typically introduced in conjunction with other materials. Of the 39 papers analyzed in this study, 25 studies combined ZIF-8 with other drugs to achieve multiple efficacies, all 25 studies [39,40,43,44,47,52,53,55–60,62–64,67,69,70,72–77] included studies

in vitro, and 12 [47,52,53,55,56,58,62,64,67,69,72,74] had animal studies that met the inclusion criteria. In 14 of the 39 papers, ZIF-8 materials were attached in the form of coatings onto titanium implants or substrates (eight papers) [41–44,47,52,67,76], magnesium alloys (two papers) [59,73], polyetheretherketone (PEEK) (two papers) [41,56], a polypropylene (PP) membrane (one paper) [45], or biphasic calcium phosphate ceramics (one paper) [50]. Other forms of ZIF-8 loading include hydrogels (10 papers) [46,51,61,64,66,69–72,74], scaffolds (four papers) [39,48,62,63], biological membranes or fibers (six papers) [40,53–55,60,75], and bone cement (one paper) [68]. Some studies [57,58,65,77] also directly use ZIF-8 nanoparticles for experiments in culture media. In addition, some ZIF-8 particles have been modified by other methods, such as polydopamine [39,49,62] or stem cell membranes (SCMs) [65,75] wrapping (Fig. 3). A total of 32 of the 39 papers [39–44,46–49,51–59,61–67,69,72,74–77] examined the release of zinc ions or drugs loaded into ZIF-8; their results show that the decomposition of ZIF-8 is pH-responsive and easier to decompose under acidic conditions, and burst release occurred at an early stage.

Applications of ZIF-8 particles include bonding to the surface of implants or substrates in the form of coatings; loading on biological membranes, fibers, or scaffolds; and doping into hydrogels or bone cement. Other drugs can be encapsulated in the pores of ZIF-8 or combined with ZIF-8, and ZIF-8 particles can also be encapsulated and modified by other materials such as polydopamine or stem cell membranes.

3.3. Cell proliferation/viability assessments

The cytotoxicity of ZIF-8 was validated in all studies, with most using CCK-8 assays (32 papers) [40–44,46–49,51,52, 54–56,58,59,61–72,74–77]; other methods include MTT assays (three papers) [39,57,60], MTS assays (two papers) [45,50], Presto Blue assay (one paper) [53], LDH assay (one paper) [47], live/dead cell staining (10 papers) [40,45,59,61,64,67,68,70,71,74], and Annexin V/PI staining (one paper) [48,51]. Most studies used at least one of these methods, and one paper [73] did not specify the detection method.

A total of 23 papers [39–41,43,47,49,53,54,56–59,62–67, 69,72,74–76] have reported the size of the ZIF-8 particles, mainly between 50 and 300 nm. Chen et al. reported the biocompatibility of ZIF-8-modified porous titanium with two different particle sizes, micro (10 μm) and nano (200–300 nm), demonstrating that nano ZIF-8 has good biocompatibility while micro ZIF-8 has obvious cytotoxicity to MG63 cells [41].

A total of 16 papers [40,42,46,49,51,55–58,61,63,65,66,68,71,77] have reported on the biocompatibility of ZIF-8 at different concentrations, of which 12 [40,46,51,55–58,63,65,66,68,69] have demonstrated the dose-dependent cytotoxicity of ZIF-8. Gao et al. found that rat bone mesenchymal stem cells (rBMSCs) cultured at 50 μg mL^{-1} nano ZIF-8 show the highest viability, with anti-apoptotic properties at concentrations below 50 μg mL^{-1} and pro-apoptotic effects at doses above 50 μg mL^{-1} [51]. Zhang et al. observed the same trend in their activity tests for rBMSCs, and also used activity tests for HUVECs to show that 75 μg mL^{-1} is the optimal activity concentration [69]. Shi et al. reported that, for ectomesenchymal stem cells (EMSCs), ZIF-8 has anti-apoptotic properties at concentrations <20 μg mL^{-1} and pro-apoptotic effects at concentrations >30 μg mL^{-1} [66]. Ge et al. found no statistically significant difference in the number of MC3T3-E1 cells in the ZIF-8 group compared to the control group at concentrations of 50 and 100 μg mL^{-1}, while noting that the number of MC3T3-E1 cells decreased significantly at concentrations of 200 μg mL^{-1} [57]. In four other studies [44,49,61,71], cell activity was not significantly different from that of the control in groups with different levels of ZIF-8. Of these studies, Chen et al. noted that PEEK coated with ZIF-8 has lower initial cell attachment than sulfonated PEEK (sPEEK), but subsequent cell proliferation is not significantly affected [49].

Table 1
Results of in vitro studies.

Author/Year	Form of materials/ Other drugs	The particle size of ZIF-8 particles	Group/treatment	Zinc ion release	Drug release	Cell type	Cell proliferation and viability assessment/ Outcomes		Cell osteogenic differentiation assessment/Outcomes		Other outcomes
Chen et al. 2017 [41]	Coated on Ti	nanoZIF-8: 10 μm; microZIF-8: 200–300 nm	Ti; AHT; nanoZIF-8; microZIF-8	nanoZIF-8: 7.36 μg mL^{-1} at 14 days; microZIF-8: 30.91 μg mL^{-1} on the first day and increased to 57.23 μg mL^{-1} on the 14th day (10% FBS-containing culture medium, 37 °C)		MG63 cells	CCK-8 assay	Decreased in the microZIF-8 group	ALP activity, Alizarin red staining, RT-PCR, ELISA (OCN)	Increased in nano ZIF-8 group	Increased antibacterial effect in nano ZIF-8 group against *S. mutans*
Zhang et al. 2017 [42]	Coated on Ti		Ti; AHT; ZIF-8@AHT-1; ZIF-8@AHT-1/2; ZIF-8@AHT-1/4; ZIF-8@AHT-1/8; ZIF-8@AHT-1/16	ZIF-8@AHT-1: 1.08 μg mL^{-1} at 12 h, 1.69 μg mL^{-1} on the 4th day; ZIF-8@AHT-1/2: 0.76 μg mL^{-1} at 12 h, 1.46 μg mL^{-1} on the 4th day; ZIF-8@AHT-1/4: 0.72 μg mL^{-1} at 12 h, 1.23 μg mL^{-1} on the 4th day; ZIF-8@ AHT-1/8: 0.56 μg mL^{-1} at 12 h, 0.96 μg mL^{-1} on the 4th day; ZIF-8@AHT-1/16: 0.24 μg mL^{-1} at 12 h, 0.39 μg mL^{-1} on the 4th day (PBS)		MC3T3-E1 cells	CCK-8 assay	No significant difference	ALP activity, Alizarin Red staining, Sirius Red staining, ELISA (OPG), RT-PCR	Increased most in the ZIF-8@AHT-1/8 group	
Ran et al. 2018 [43]	Coated on Ti (Dexamethasone)	ZIF-8: 60 nm	Pristine Ti; The SF-ZIF-8-Ti; The SF-DEX@ZIF-8-Ti		DEX@ZIF-8: DEX released over the 10 days; SF-DEX@ZIF-8-Ti: DEX released over the 30 days (PBS, pH 7.4, 37 °C)	MC3T3-E1 cells	CCK-8 assay	No significant difference	ALP activity, Alizarin red staining, qRT-PCR	Increased in SF-DEX@ZIF-8-Ti group, but didn't in SF-ZIF-8-Ti group	
Zhang et al. 2019 [44]	Coated on Ti (Dimethyloxalyl glycine)		Blank; Pure Ti; Z-AHT; D-AHT	Release percentage: 65.7% for Z-AHT and 65.6%	90.5% DMOG was released in the first 24 h and reached a	MC3T3-E1 cells, HUVEC	CCK-8 assay	Increased in Ti, Z-AHT, and D-AHT groups	ALP activity, RT-PCR	Increased similarly in Z-AHT and D-AHT groups	The trend of HUVEC migration is D-

(*continued on next page*)

Table 1 (*continued*)

Author/Year	Form of materials/ Other drugs	The particle size of ZIF-8 particles	Group/treatment	Zinc ion release	Drug release	Cell type	Cell proliferation and viability assessment/ Outcomes		Cell osteogenic differentiation assessment/Outcomes		Other outcomes
				for D-AHT on the first 12 h; Final concentration: Z-AHT and D-AHT was 0.87 ± 0.01 µg mL^{-1} and 0.83 ± 0.02 µg mL^{-1} on day 7 (PBS, 37 °C)	concentration of 0.53 ± 0.01 µg mL^{-1}; 0.56 ± 0.02 µg mL^{-1} at 48 h; 0.59 ± 0.02 µg mL^{-1} at 96 h (PBS, 37 °C)						AHT > Z-AHT > Ti
Ejeian et al. 2020 [45]	Coated on polypropylene membrane		Tissue culture plates (TCP); PP/PDA/ZIF-8 substrate			DPSCs	MTS assay, live/ dead cell staining	Increased on ZIF-8 layer	qRT-PCR, immunofluorescence staining	Increased in PP/PDA/ZIF8 group	
Liu et al. 2020 [46]	Contained in CA-CS hydrogel		CA-CS/ZL (CA-CS/ ZIF-8 = 50:1 w/w); CA-CS/ZM (CA-CS/ ZIF-8 = 25:1 *w*/w); CA-CS/ZH (CA-CS/ ZIF-8 = 15:1 w/w); CA-CS	CA-CS/ZL: 0.39 µg mL^{-1} at 6 h; 0.57 µg mL^{-1} at 7 days; CA-CS/ZM: 0.62 µg mL^{-1} at 6 h, 0.94 µg mL^{-1} at 7 days; CA-CS/ZH: 0.89 µg mL^{-1} at 6 h, 1.78 µg mL^{-1} at 7 days; After 1 day, the release rate decreased slowly (PBS, 37 °C)		rBMSCs, HUVECs	CCK-8 assay	Increased in CA-CS, CA-CS/ZL, and CA-CS/ZM groups, especially in CA-CS/ZM group	ALP activity, Sirius Red stain, Alizarin red stain, RT-PCR, Western Blot	Increased in CA-CS, CA-CS/ ZL, and CA-CS/ ZM groups, especially in CA-CS/ZM group	Increased angiogenic effects in CA-CS/Z groups, especially in CA-CS/ZM group; the highest antibacterial effect against *E. coli* and *S. aureus* in CA-CS/ZM
Tao et al. 2020 [47]	Coated on Ti (Levofloxacin)	MOF: 136 ± 28 nm; MOF@Levo: 189 ± 35 nm	Ti; Col I; MOF; MOF@Levo; MOF@Levo/LBL	At 240 h in PBS, 37 °C MOF: 3.89 mg L^{-1} (pH 7.4), 6.4 mg L^{-1} (pH 5.5); MOF@Levo: 3.91 mg L^{-1} (pH 7.4), 6.5 mg L^{-1} (pH 5.5); MOF@Levo/ LBL: 2.59 mg L^{-1} (pH 7.4), 4.7 mg L^{-1} (pH 5.5)	After incubation for 24 h: MOF@Levo/ LBL: 15.9 µg Levo at pH 7.4, 35.3 µg Levo at pH 5.5; MOF@Levo: 23.1 µg Levo at pH 7.4; After incubation for 10 days: MOF@Levo/ LBL: 47.2 at pH 7.4 and 106.7 µg Levo at pH 5.5; The final quantity of Levo in MOF@Levo/	Osteoblasts derived from the calvaria of neonatal rats	CCK-8 assay, LDH assay	Decreased in MOF and MOF@Levo groups, but increased in MOF@Levo/ LBL group	ALP activity, Sirius Red staining, Alizarin Red S staining, RT-PCR	Increased in MOF@Levo/ LBL group, but didn't in MOF and MOF@Levo groups	Increased antibacterial effects against *E. coli* and *S. aureus* in MOF, MOF@Levo, and MOF@Levo/ LBL groups

Table 1 (*continued*)

Author/Year	Form of materials/ Other drugs	The particle size of ZIF-8 particles	Group/treatment	Zinc ion release	Drug release	Cell type	Cell proliferation and viability assessment/ Outcomes		Cell osteogenic differentiation assessment/Outcomes		Other outcomes
Zhong et al. 2020 [48]	Contained in PCL/DCPD scaffold		Pure PCL scaffold; PCL/DCPD scaffold; PCL/DCPD/ nanoZIF-8 scaffold (0.5 wt% nanoZIF-8)	During the first 5 days, the concentration of Zn ions dramatically increased, while the upward trend remained much steadier afterward. (Tris-HCl buffer, pH 7.4, 37 °C)	LBL was approximately 118.9 μg.	rBMSCs	CCK-8 assay, Annexin V/PI staining	No significant difference	RT-qPCR, Western Blot, ELISA, Alizarin Red S staining	Increased most in PCL/DCPD/ nano ZIF-8 group	
Chen et al. 2021 [49]	Coated on PEEK	ZIF-8: 130–200 nm	sPEEK; Z-1/sPEEK (by 100 μg mL^{-1} ZIF-8 solution); Z-3/sPEEK (by 200 μg mL^{-1} ZIF-8 solution)	Z-1/sPEEK: 0.07 μg mL^{-1} at 144 h; Z-3/sPEEK: 0.154 μg mL^{-1} at 144 h (PBS, 37 °C)		MC3T3-E1 cells	CCK-8 assay	No significant difference, but lower initial cell attachment on coating with ZIF-8	ALP activity, Alizarin Red S staining,	Increased most in the Z-3/ sPEEK group	Polydopamine-wrapped ZIF-8 coating possesses bactericidal efficiencies of 100% against *S. aureus* and *E. coli* under NIR
Fardjahromi et al. 2021 [50]	Coated on BCPs		Osteon; ZIF-8 Osteon			hADSCs	MTS assay	Increased in ZIF-8 Osteon group	Immunofluorescence staining, Alizarin Red S staining, qRT-PCR	Increased in the ZIF8-Osteon group	
Gao et al. 2021 [51]	In vitro: nanoparticles contained in DMEM media; In vivo: contained in SA hydrogel		Proliferation, viability, and osteogenic differentiation: control; 10 μg mL^{-1} nano ZIF-8; 25 μg mL^{-1} nano ZIF-8; 50 μg mL^{-1} nano ZIF-8; 75 μg mL^{-1} nano ZIF-8; 100 μg mL^{-1} nano ZIF-8 Osteogenic differentiation: control; zinc sulfate; nano ZIF-8 (50 μg mL^{-1}); dimethylimidazole	A rapid and small release of Zn^{2+} occurred on the first day, followed by a stable linear release from the solution. After 4 days, the concentration of Zn^{2+} ions in the solution remained stable (DMEM)		rBMSCs	CCK-8 assay, Annexin V/PI staining	Increased on nano ZIF-8 at concentrations <50 μg mL^{-1}, and decreased at above 50 μg mL^{-1}; cells cultured with 25 (day 1) and 50 μg mL^{-1} (day 5) nano ZIF-8 showed the highest viability	ALP activity, Alizarin Red S staining, RT-PCR, Western Blot	Increased in 10, 25, 50, and 75 μg mL^{-1} nano ZIF-8 groups, especially in the 50 μg mL^{-1} group; increased in the zinc sulfate group and nano ZIF-8 group, especially in the nano ZIF-8 group	
Jiang et al. 2021 [39]	Contained in gelatin scaffold	pZIF-8: 50 nm	Bare-G; pZIF-8-G;		20% of BMP-2 was released in	BMSCs	MTT assay	Increased on NP-assembled-	ALP activity, RT-qPCR	Increased in BMP-2-pZIF-8/	

Table 1 (*continued*)

Author/Year	Form of materials/ Other drugs	The particle size of ZIF-8 particles	Group/treatment	Zinc ion release	Drug release	Cell type	Cell proliferation and viability assessment/ Outcomes		Cell osteogenic differentiation assessment/Outcomes		Other outcomes
	(Hydroxyapatite, BMP-2)		pHA-G; pZIF-8/pHA-G; BMP-2-loaded pZIF-8/pHA-G		the first 7 days, and 40% of BMP-2 was released after 21 days. (PBS, pH 7.4)			scaffolds, especially in BMP-2-loaded pZIF-8/pHA-G group	qRT-PCR	pHA-G group, but didn't in pZIF-8-G group	
Teng et al. 2021 [52]	Coated on Ti (Iodine)		TC4; MAO; MAO + Z; MAO + ZI	Zinc release from ZIF-8 was pH-responsive. (SBF, pH 7.4 and 6.0)	Iodine Zinc release from ZIF-8 was pH-responsive. (SBF, pH 7.4 and 6.0)	hBMSCs	CCK-8 assay	No significant difference	qRT-PCR	Increased in MAO, MAO + Z and MAO + ZI groups, especially in MAO + ZI group	Increased antibacterial effects against *S. aureus* in MAO, MAO + Z, and MAO + ZI groups, especially in the MAO + ZI group and after NIR exposure
Toprak et al. 2021 [53]	Contained in electrospun PCL/ZIF-8 membrane (BMP-6)	ZIF-8: 83 nm ± 18; BMP@ZIF-8: 68 nm ± 15	PCL; PCL/ZIF-8; PCL/BMP@ZIF-8		12% at 4 h; 35% at 30 days (PBS, pH 7.4, 37 °C)	MC3T3-E1 cells	Presto Blue assay	Increased in PCL/BMP@ZIF-8 group	ALP activity, Alizarin Red S staining, qRT-PCR	Increased in PCL/BMP-6@ZIF-8 group, but decreased in PCL/ZIF-8 group	
Xue et al. 2021 [54]	Loaded on electrospun PCL/Col membrane	ZIF-8: 300 nm	Col; PCL/Col; ZIF-8 crystal layer (of PCL/Col/ZIF-8 composite membrane)	There was a small, acute release in the first 24 h, and then the release gradually slowed afterward; 1.54 ± 0.05 μg mL^{-1} on the 7th day (culture medium, pH 7.4); 93% ions were released from the PCL/Col/ZIF-8 composite membrane within 12 h (culture medium, pH 5.5)		rBMSCs, HUVECs	CCK-8 assay	Increased on ZIF-8 crystal layer	ALP activity, Alizarin Red S staining, RT-PCR	Increased on ZIF-8 crystal layer	Increased angiogenic effect in ZIF-8 crystal layer group
Al-Baadani et al. 2022 [55]	Loaded on polycaprolactone/ gelatin blended membrane (Alendronate)		PG; PG/ZIF-8(0.25%); PG/ZIF-8(0.5%); PG/ZIF-8(1%); PG/Aln; PG/Aln-ZIF-8 (0.25%); PG/Aln-ZIF-8	An initial burst release in the first two days: PG/ZIF-8 (0.25%), PG/ZIF-8(0.5%), PG/ZIF-8(1%) groups were	On the 4th day, an initial burst release of Aln from the PG/Aln group (24 μg/cm2); PG/Aln-ZIF-8 (0.25%), PG/	MC3T3-E1 cells, RAW 264.7	CCK-8 assay	Decreased in the PG/ZIF-8 (0.5%) and PG/ZIF-8(1%) groups, especially in the PG/ZIF-8(1%) group	ALP activity, Alizarin Red staining, Sirius Red staining, RT-qPCR	Increased in PG/ZIF-8 (0.25%) and PG/ZIF-8 (0.5%), especially in the PG/ZIF-8 (0.25%) group,	The number of osteoclasts decreased gradually with the increase of ZIF-8 concentration; the colonies

Table 1 (*continued*)

Author/Year	Form of materials/ Other drugs	The particle size of ZIF-8 particles	Group/treatment	Zinc ion release	Drug release	Cell type	Cell proliferation and viability assessment/ Outcomes		Cell osteogenic differentiation assessment/Outcomes		Other outcomes
			(0.5%); PG/Aln-ZIF-8(1%)	0.44, 0.85, and 1.34 µg cm^{-2}, respectively; PG/Aln-ZIF-8 (0.25%), PG/ Aln-ZIF-8 (0.5%), and PG/ Aln-ZIF-8(1%) groups, were 0.18, 0.56 and 1.31 µg cm^{-2}, respectively (PBS, pH 7.4)	Aln-ZIF-8 (0.5%), and PG/ Aln-ZIF-8(1%) groups were about 5 µg/cm^2 (PBS, pH 7.4)				decreased in PG/ZIF-8(1%) group	numbers of *S. aureus* and *E. coli* decreased in a ZIF-8 concentration-dependent manner
Deng et al. 2022 [56]	Coated on PEEK (Simvastatin)	100–200 nm	sPEEK; Z-sP (100 µg mL^{-1}); Z3-sP (300 µg mL^{-1}); S@Z-sP; S@Z3-sP	About 0.07 and 0.15 µg mL^{-1} in S@Z-sP and S@Z3-sP groups at 144 h, respectively	A visible burst release during the early stage (<48 h)	MC3T3-E1 cells	CCK-8 assay	Compared with the sPEEK group, the S@Z3-sP group increased after 5 days, but other groups were decreased	ALP activity, Alizarin Red S staining, qRT-PCR	Increased in all the groups, especially in the S@Z3-sP group	
Ge et al. 2022 [57]	Nanoparticles contained in PBS (Celecoxib)	ZIF-8: 365 ± 4 nm; CEL@ZIF-8: 372 ± 10 nm	Proliferation and viability: ZIF-8 at different concentrations (0, 50, 100, and 200 µg mL^{-1}); CEL@ZIF-8 at different concentrations (0, 50, 100, and 200 µg mL^{-1}) Osteogenic differentiation: Control; ZIF-8 (100 µg mL^{-1}); CEL@ZIF-8 (100 µg mL^{-1})	The release of ions is very slow at pH 7.4, while the release rate and cumulative amount of ions increase significantly at pH 6.0 and 5.0, and both increase more significantly at pH 5.0 (PBS, 37 °C)	Released rate after 72 h: 27.53 + 3.22% at pH 7.4; 78.02% ± 1.97% at pH 6.0; 95.32 + 4.76% at pH 5.0 (PBS, 37 °C)	MC3T3-E1 cells	MTT assay	No significant difference at concentrations of 0, 50, and 100 µg mL^{-1}, but decreased at a concentration of 200 µg mL^{-1}	qPCR, ALP staining, Alizarin Red S staining,	Increased in all experimental groups	Increased antibacterial effects against *S. aureus* and E. coli in CEL@ZIF-8 and ZIF-8 groups; significant decrease in all inflammatory factors in both CEL@ZIF-8 and ZIF-8 groups, especially the CEL@ZIF-8 group
Liang et al. 2022 [58]	In vitro: nanoparticles contained in a normal medium In vivo: nanoparticles contained in the mixture of Matrigel and PBS (Dexamethasone)	ZIF-8: 100 nm	Proliferation and viability: ZIF-8 at differentiation concentrations (25, 50, and 100 µg mL^{-1}) Proliferation, viability, and osteogenic differentiation: Control (no		In the first 12 d, the release was relatively quick, followed by a slow release phase until the final volume released reached 78% after 24 d (PBS, 37 °C)	MSCs	CCK-8 assay	Decreased dramatically at the concentrations of 50 and 100 µg mL^{-1}; increased in the DEX@ZIF-8-SCM group	ALP Assay, q-PCR, immunofluorescence staining, Alizarin Red S staining	Increased in DEX@ZIF-8 and DEX@ZIF-8-SCM groups, but didn't in ZIF-8 group	

(*continued on next page*)

Table 1 (continued)

Author/Year	Form of materials/ Other drugs	The particle size of ZIF-8 particles	Group/treatment	Zinc ion release	Drug release	Cell type	Cell proliferation and viability assessment/ Outcomes		Cell osteogenic differentiation assessment/Outcomes		Other outcomes
			nanoparticles); ZIF-8 (25 µg mL^{-1}); DEX@ZIF-8 (25 µg mL^{-1}); DEX@ZIF-8-SCM (25 µg mL^{-1})								
Ling et al. 2022 [59]	Coated on Mg alloy (Hydroxyapatite)	Cu@ZIF-8: 0.364 µm - 1.646 µm	Bare Mg alloy; HA; ZIF-8/HA; Cu15@ZIF-8/HA (15% copper); Cu30@ZIF-8/HA (30% copper); Cu45@ZIF-8/HA (45% copper)	Cu45@ZIF-8/ HA: Copper and zinc ions reached almost saturation after 7 days of immersion, with a 7-day release of 881.56 and 456.48 µg L^{-1} (SBF, 37 °C)		MC3T3-E1 cells	CCK-8 assay, live/ dead cell staining	Increased on ZIF-8 modified specimens, especially on Cu45@ZIF-8/ HA	ALP activity	Increased in ZIF-8 modified groups, especially on Cu45@ZIF-8/ HA	Cu@ZIF-8/HA composite coatings showed excellent antibacterial ability against *S. aureus* and *E. coli*.
Liu et al. 2022 [60]	Loaded on electrospun PCL/lignin nanofiber (Lignin)		PCL; PCL/LIG; PCL/ZIF-8; PCL/LIG/ZIF-8			rBMSCs	MTT assay	Increased in PCL/LIG, PCL/ ZIF-8, and PCL/ LIG/ZIF-8 groups, especially on PCL/LIG/ZIF-8 group	ALP activity, Alizarin Red S staining, RT-qPCR	Increased trend is PCL < PCL/ LIG < PCL/ZIF-8 < PCL/LIG/ ZIF-8	PCL/ZIF-8 and PCL/LIG/ZIF-8 composite nanofibers had an inhibition rate against *E. coli* and *S. aureus* that almost reached 100%
Liu et al. 2022 [61]	Contained in gelatin methacryloyl hydrogel		GelMA; GelMA-ZL (0.05% *w/v*); GelMA-ZM (0.1% *w/v*); GelMA-ZH (0.2% w/v)	GelMA-ZL: 0.49 µg mL^{-1} at 24 h, 0.72 µg mL^{-1} after 14 d; GelMA-ZM: 0.62 µg mL^{-1} at 24 h, 0.94 µg mL^{-1} after 14 d; GelMA-ZH: 0.91 µg mL^{-1} at 24 h, 1.25 µg mL^{-1} after 14 d (PBS, pH 7.4, 37 °C)		rBMSCs	CCK-8 assay, live/ dead cell staining	No significant difference	ALP activity, Alizarin Red S staining, RT-qPCR	Increased in all GelMA-Z groups, especially in the GelMA-ZH group	Increased antibacterial effect against *P. gingivalis* in GelMA-ZH group
Ni et al. 2022 [62]	Contained in COL hydrogel and perfused into PLGA-TCP scaffold (Platelet-derived growth factor)	ZIF-8-PDA: 226.2 ± 5.3 nm	Tissue culture polystyrene (TCPS) plates; PLGA-TCP scaffolds; ZIF-8-PDA@COL/ PLGA-TCP scaffolds; PDGF@ZIF-8-PDA@COL/ PLGATCP scaffolds		After 28 h: PDGF@ZIF-8-PDA@COL/ PLGA-TCP composite scaffolds: 43.28 ± 2.45% of PDGF; PDGF@ COL/ PLGA-TCP scaffolds: 78. 95 ± 2.41% of	MSCs	CCK-8 assay	Increased in ZIF-8-PDA@COL/ PLGA-TCP and PDGF@ZIF-8-PDA@COL/ PLGA-TCP groups	ALP activity, Alizarin Red S staining, RT-qPCR	Increased in ZIF-8-PDA@COL/ PLGA-TCP and PDGF@ZIF-8-PDA@COL/ PLGA-TCP groups, especially in the PDGF@ZIF-8-PDA@COL/	Increased antibacterials effects against *E. coli* and *S. aureus* in ZIF-8-PDA@COL/ PLGA-TCP groups with or without PDGF, especially with NIR irradiation

Table 1 (*continued*)

Author/Year	Form of materials/ Other drugs	The particle size of ZIF-8 particles	Group/treatment	Zinc ion release	Drug release	Cell type	Cell proliferation and viability assessment/ Outcomes		Cell osteogenic differentiation assessment/Outcomes	Other outcomes
Pan et al. 2022 [63]	Loaded on gelatin nanofibrous scaffold (Phenamil)	ZIF-8: 56.77 ± 13.98 nm	Proliferation and viability: ZIF-8 at different concentrations (0 µg mL^{-1}, 100 µg mL^{-1}, 200 µg mL^{-1}, 300 µg mL^{-1}) Osteogenic differentiation: GF; GF/BMP2; GF/2ZIF8-Phe (200 µg mL^{-1}); GF/2ZIF8-Phe/ BMP2 (200 µg mL^{-1})		PDGF (PBS, pH 7.4) Burst release on all three types of groups; BMP2 was completed and released from the GF scaffolds in 72 h; The application of NIR to GF/ 2ZIF8-Phe accelerated Phe release compared to the NIR untreated group. (DPBS, 37 °C)	C2C12	CCK-8 assay	Increased at the concentration lower than 200 µg mL^{-1}	ALP activity	PLGA-TCP group Increased in GF/BMP2 and GF/2ZIF8-Phe/ BMP2 groups, especially in GF/2ZIF8-Phe/ BMP2 group
Qiao et al. 2022 [64]	Contained in the PEGDA/SA hydrogel (Simvastatin)	SIM@ZIF-8: 100–200 nm	PS; nZPS; nSZPS (nano SIM@ZIF-8/ PEGDA/SA)	Both nZPS and nSZPS groups had relatively acute Zn^{2+} release in the first 24 h, and the release rate slowly decreased after 3 d. By the 8th day, the release rate of Zn^{2+} became stable	The release curve of SIM was similar to that of Zn^{2+} from SIM@ZIF-8	BMSCs	CCK-8 assay, live/ dead cell staining	No significant difference	ALP activity, Alizarin Red S staining, RT-qPCR, Western blot	Increased in nZPS and nSZPS groups, especially in the nSZPS group
Ren et al. 2022 [65]	In vitro: nanoparticles contained in a normal medium In vivo: nanoparticles contained in the mixture of Matrigel and PBS	ZIF-8: 100 nm	Proliferation and viability: ZIF-8 and SCM/ ZIF-8 at different concentrations (25 µg mL^{-1} and 50 µg mL^{-1}) Osteogenic differentiation: Control; ZIF-8 (25 µg mL^{-1}); SCM/ZIF-8 (25 µg mL^{-1})	Zn^{2+} were drastically released from both ZIF-8 and SCM/ZIF-8 in a relatively stable linear trend;the wrapped SCM inhibited the excessively fast release of Zn^{2+} (PBS, 37 °C)		MSCs	CCK-8 assay	Increased in ZIF-8 and SCM/ ZIF-8 groups at 25 µg mL^{-1}, especially SCM/ ZIF-8 groups	ALP activity, Alizarin Red S staining, qPCR, immunofluorescence staining,	The increased trend is SCM/ ZIF-8 > ZIF-8 > Control
Shi et al. 2022 [66]	Contained in fibrin hydrogels (but nanoparticles contained in a medium were used for viability assessment)	ZIF-8: 200 nm	Proliferation and viability, and osteogenic differentiation: ZIF-8 at different concentrations (10,	Nanoparticles: Rapid release of a small amount of Zn^{2+} occurred on the first day; after 9		EMSCs	CCK-8 assay	ZIF-8 has antiapoptotic properties at concentrations <20 µg mL^{-1} and	ALP assays, Alizarin Red S staining, Western Blot, immunofluorescence staining	Nanoparticles: increased most at 20 µg mL^{-1} Hydrogels: increased most

Table 1 (*continued*)

Author/Year	Form of materials/ Other drugs	The particle size of ZIF-8 particles	Group/treatment	Zinc ion release	Drug release	Cell type	Cell proliferation and viability assessment/ Outcomes		Cell osteogenic differentiation assessment/Outcomes		Other outcomes
			20, 30, 40, 50, 100 µg mL^{-1}) Osteogenic differentiation (Hydrogels): FG (Fibrin gel); Z10-FG (10 µg mL^{-1}); Z20-FG (20 µg mL^{-1})	days, the concentration of Zn^{2+} ions in the solution remained stable; Hydrogels: Z10-FG: 1.1 µg mL^{-1}; Z20-FG: 1.3 µg mL^{-1}; Z150-FG: 4.5 µg mL^{-1} (Rat blood plasma or DMEM/F12, pH = 7.35, 37 °C)				proapoptotic effects at concentrations >30 µg mL^{-1}		in the Z20-FG group	
Sun et al. 2022 [40]	Loaded in the PVP part of PCL/PVP Janus nanofiber membrane (Tacrolimus (FK506))	ZIF-8: 110.58 ± 9.39 nm	Proliferation and viability: ZIF-8 at different concentrations (0.5 wt%, 1 wt%, 1.5 wt% and 2 wt%) Proliferation, viability, and osteogenic differentiation: PP JNF; PPZ JNF (1 wt%); PPF JNF; PPZF JNF (1 wt%)	There was a small, acute release of Zn^{2+} on the first day from PPZ JNF and PPZF JNF. Afterward, the release rate gradually slowed down during days 1 to 7. (PBS, 37 °C)	The nanofibers loaded with FK506 exhibited a burst release in the first 6 h, and then a secondary, slower nonlinear release. (PBS, 37 °C)	BMSCs	CCK-8 assay, Cell live/ dead staining,	Increased most in 1 wt% ZIF-8 group; no significant difference	ALP assays, Alizarin Red S staining, RT-qPCR, Western Blot	The increased trend is PP JNF < PPF JNF < PPZ JNF < PPZF JNF	Increased antibacterial effects against *E. coli* and *S. aureus* in PPZ and PPZF JNF groups
Wang et al. 2022 [67]	Coated on Ti (Naringin)	ZIF-8: 176.2 nm; ZIF-8@Nar: 178.6 nm	Ti; TNT; TNT-ZIF-8; TNT-ZIF-8@Nar	At a pH value of 5.5: TNT-ZIF-8: 0.92 ppm on day 1; TNT-ZIF-8@Nar: 0.98 ppm on day 1, 2.02 ppm on day 7 At a pH value of 7.4: the release of Zn^{2+} from the MOF-modified Ti substrates slowed and then continuously released for 14	The total amount of Nar loaded and released from TNT-ZIF-8@Nar was 9.12 and 8.67 µg (PBS, 37 °C)	Osteoblasts isolated from calvaria of neonatal rats	CCK-8 assay, Cell live/ dead staining,	Decreased in TNT-ZIF-8 group, but increased most in TNT-ZIF-8@Nar group	ALP assay, Sirius Red staining, Alizarin Red S staining, qRT-PCR	Increased in TNT-ZIF-8@Nar group, but didn't in TNT-ZIF-8 group	Increased antibacterial effects against *E. coli* and *S. aureus* in MOF-modified Ti groups

Table 1 (*continued*)

Author/Year	Form of materials/ Other drugs	The particle size of ZIF-8 particles	Group/treatment	Zinc ion release	Drug release	Cell type	Cell proliferation and viability assessment/ Outcomes		Cell osteogenic differentiation assessment/Outcomes		Other outcomes
				days (PBS, 37 °C)							
Wang et al. 2022 [68]	Contained in bone cement		Proliferation and viability (the extracts of ZIFMPCs at 25 mg mL^{-1}): ZIF-8 at different concentrations (0, 0.5, 1.0, 3.0, and 5.0 wt%) Osteogenic differentiation: Blank; MPC; 3.0ZIFMPC (3.0 wt %)			mBMSCs	CCK-8 assay, Cell live/ dead staining,	Increased most in 3 wt%ZIF-8 group	ALP assays, Alizarin Red S staining, RT-qPCR	Increased most in the ZIFMPC group	
Zhang et al. 2022 [69]	In vitro: contained in the medium; In vivo: contained in SA hydrogel (Dimethyloxallyl glycine)	ZIF-8: 75.4 ± 9.5 nm PD@ZIF-8: 67.9 ± 10.9 nm OD@ZIF-8: 69.3 ± 11.7 nm	Proliferation and viability: ZIF-8 and DMOG@ZIF-8 at different concentrations (0, 25, 50, 75, 100 μg mL^{-1}) Osteogenic differentiation: Control (1 mL of medium with no particle was added); ZIF-8; PD@ZIF-8 (50 μg mL^{-1}); OD@ZIF-8 (50 μg mL^{-1})	On the 7th day ZIF-8: 10.81 μmol mL^{-1}; PD@ZIF-8: 9.55 μmol mL^{-1}; OD@ZIF-8: 7.82 μmol mL^{-1} (PBS, 37 °C)	OD@ZIF-8: similar to the Zn^{2+} release pattern; PD@ZIF-8: burst release in the first half day, with 62.7% (PBS, 37 °C)	BMSCs, HUVECs	CCK-8 assay	Increased most in the 50 μg mL^{-1} group for BMSCs and the 75 μg mL^{-1} group for HUVECs	ALP assays, Alizarin Red S staining, RT-qPCR, Western blot	The increased trend is the control<ZIF-8 < PD@ZIF-8 < OD@ZIF-8	OD@ZIF-8 showed the highest angiogenic activity, followed by the PD@ZIF-8, ZIF-8, and control groups
Chen et al. 2023 [70]	Contained in polyacrylamide-carboxymethylcellulose hydrogel (alendronate)		Blank; PAM-CMC; PAM-CMC@ZIF-8; PAM-CMC-10% Aln@ZIF-8			rBMSCs	CCK-8 assay, the calcein-AM/PI staining	Increased in all experimental groups, especially PAM-CMC-10% Aln@ZIF-8 group	ALP assay, Alizarin Red S staining, RT-PCR, immunostaining	Increased in all experimental groups, especially PAM-CMC-10% Aln@ZIF-8 group	
Hu et al. 2023 [71]	Contained in hydrogel that integrates poly (vinyl alcohol), L-dopa amino acid, and ZIF-8		Control; PVA; L-DP; L-DPZ1; L-DPZ2			rBMSCs	CCK-8 assay, Live/ Dead assay	No significant difference	ALP staining and Alizarin Red staining, RT-PCR	Increased in L-DPZ1 and L-DPZ2 groups, especially in L-DPZ2 group	
Lao et al. 2023 [72]	Contained in GelMA hydrogel (metformin)	ZIF-8: 80–100 nm;	GelMA-LG (low-glucose); GelMA-HG (high-	A quicker release of Zn ions in the early		BMSCs	CCK-8 assay	Compared with the GelMA-HG group, an	ALP assay, RT-PCR	Compared with the GelMA-HG group, an	

Table 1 (*continued*)

Author/Year	Form of materials/ Other drugs	The particle size of ZIF-8 particles	Group/treatment	Zinc ion release	Drug release	Cell type	Cell proliferation and viability assessment/ Outcomes	Cell osteogenic differentiation assessment/Outcomes		Other outcomes
		Met@ZIF-8: 120–160 nm	glucose); GelMA/Metformin-HG; GelMA/ZIF-8-HG; GelMA/Met@ZIF-8-HG	3 days; under an acidic environment, MOF nanoparticles showed a faster speed of Zn ions and medicine release than the neutral environment			increase in GelMA/ZIF-8-HG group		increase in GelMA/ZIF-8-HG group	
Li et al. 2023 [73]	Coated on Mg alloy (Ag)		MAO; Ag/LDH (layered double hydroxide); Ag/ZIF-8/LDH			MC3T3-E1 cells, rBMSCs	The cell viabilities of the Ag/LDH and Ag/ZIF-8/LDH groups exceeded 88% after 1 day, 2 days, and 3 days of incubation	ALP activity, RT-PCR	Increased most in Ag/ZIF-8/LDH group	
Li et al. 2023 [74]	In vitro: nanoparticles In vivo: contained in sodium alginate hydrogel (deferoxamine)	ZIF-8: 150 nm; DFO@ZIF-8: 200 nm	Con; DFO; ZIF-8; DFO @ZIF-8	On the 10th day: ZIF-8 was 8.42 μg mL^{-1} DFO@ZIF-8 was 7.19 μg mL^{-1}		BMSCs, HUVECs	CCK-8 assay, Live/dead staining	Both HUVECs and BMSCs exhibited the increased trend is Con < DFO < ZIF-8 < DFO @ZIF-8	ALP assay, Alizarin red staining, RT-PCR, ELISA	The increased trend is Con < DFO < ZIF-8 < DFO @ZIF-8	The promoted angiogenesis trend is Con < ZIF-8 < DFO < DFO @ZIF-8
Shu et al. 2023 [75]	Loaded in PCL/PLA membrane (Hydroxyapatite)	ZIF-8: 117 nm	Blank; PCL/PLA; 30% n-HA; 5% ZIF-8 (with 30% n-HA); 5% Cu@ZIF-8 (with 30% n-HA)	In one week, 3.4 ppm of Zn ion and 5.8 ppm of Cu ion were released; a total of 4.2 ppm of Zn ion and 7.5 ppm of Cu ion released after 35 days (PBS, pH 7.4, 37 °C)		BMSCs	CCK-8 assay	Increased in 30% n-HA and 5% ZIF-8 groups, but no difference between in 5% Cu@ZIF-8 and blank groups	ALP assays, Alizarin Red S staining	Increased in n-HA, ZIF-8, and Cu@ZIF-8 groups, especially in Cu@ZIF-8	Increased antibacterial effects against *E. coli* and *S. aureus* in 5% ZIF-8 and 5% Cu@ZIF-8 groups, especially in the 5% Cu@ZIF-8 group
Si et al. 2023 [76]	Coated on Ti (methyl vanillate)	400 nm	Ti; TO; TOP; TOPZ; TOPMZ	About 6.5 μg mL^{-1} after 20 days (PBS, 37 °C)		hBMSCs	CCK-8 assay	No statistical difference was noticed betwixt the TOPZ and Ti at day 5	ALP assay, RT-qPCR, Alizarin Red S staining, Western blot assay, immunofluorescence staining,	The increased trend is TOP < TOPZ < TOPMZ	MV and ZIF-8 exhibits enhanced antibacterial properties
Xu et al. 2023 [77]	Nanoparticles (resveratrol)		RSV; ZIF-8/RSV; ZIF-8; Control		When the pH decreased from 7.4 to 5.5, the cumulative release of RSV increased from 10.3 to 94.6% (PBS)	Human osteoblasts (HOBs)	CCK8 assay	Increased in the ZIF-8/RSV group, but decreased in the ZIF-8 group	ALP assay, qRT-PCR	Increased in the ZIF-8/RSV group, but decreased in the ZIF-8 group	

3.4. Cellular osteogenic differentiation and vascularization tests assessments

All papers included in this review assessed cellular osteogenic differentiation. Of these 39 papers, 35 [39–44,46,47,49,51,53–77] evaluated alkaline phosphatase (ALP) activity, 30 [40,41,43,46–51,53–58,60–62,64–71,74–77] evaluated extracellular matrix mineralization by Alizarin Red staining, 34 papers [39–48,50–58,60–62,64,65,67–74,76,77] evaluated the expression of osteogenesis-related genes by PCR, and seven, seven, five, and four papers evaluated the production and release of osteoblast-associated proteins and markers by Western Blot [40,48,51,64,66,69,76], immunofluorescence staining [45,50,58,65,66,70,76], Sirius Red staining [42,46,47,55,67], and ELISA [41,42,48,74] respectively. Overall, ZIF-8 has been proven to significantly promote osteogenic differentiation.

Seven papers of 39 papers [42,46,49,51,55,61,71] compared the osteogenic properties of ZIF-8 at different concentrations and found that these properties are dose-dependent. Gao et al. found that rBMSCs cultured at 50 µg mL^{-1} nano ZIF-8 exhibit the highest ALP activity; Gao et al. [51] also showed that zinc sulfate with an equivalent molar mass concentration of Zn^{2+} to nano ZIF-8 promotes osteogenic differentiation and stimulates the expression of osteogenesis-related genes and proteins, which was slightly inferior to nano ZIF-8, while dimethylimidazole has little effect on osteogenesis in rBMSCs. In subsequent animal experiments on maxillary defect models, SA/micro ZIF-8 at a concentration of 35 µg mL^{-1} was introduced into the experiment because it releases Zn^{2+} at the same rate as SA/nano ZIF-8 early in osteogenesis, but the protein expression response is also relatively low.

In 25 studies, ZIF-8 was used in combination with other drugs; all of these studies reported that the addition of ZIF-8 improved the osteogenesis-related parameters of the material. However, five papers [39,43,47,58,67] reported that in the experimental group with only ZIF-8, the difference in osteogenesis-related parameters between the ZIF-8 group and the control group was not significant, and in two papers [53,77] some osteogenesis-related parameters in the experimental group with only ZIF-8 were lower than those in the control group.

Five studies [44,46,54,69,74] investigated the angiogenesis of ZIF-8 materials, where ZIF-8 shows good vasogenic activity at appropriate doses.

3.5. In vivo experiments

Of the 22 available animal trials, the animals included SD rats (14 papers) [46,47,51,52,54–56,62,64,66,67,69,72,74], Wistar rats (four papers) [53,58,61,65], New Zealand rabbits (three papers) [48,50,71], and mice (one paper) [42]. Bone defects were mainly located in the skull (15 papers) [46,48,50,53–56,62,64,66,67,69,71,72,74], femur (four papers) [47,58,65,67], maxilla (three papers) [42,51,61], and tibia (one paper) [52]. All studies showed that appropriate concentrations of ZIF-8 can promote bone formation, which is consistent with the results of the in vitro studies.

4. Discussion

4.1. Degradation characteristics of ZIF-8 material

ZIF-8 is a bone tissue engineering material, which has been increasingly studied in recent years, and it is a porous network assembled by coordination interactions between ligand (2-methylimidazole) linkers and metal ions (Zn^{2+}). Zhang et al. summarized the dissolution of ZIF-8 structure in aqueous solution in the following steps: (1) 2-methylimidazole ligands, the terminal group in ZIF-8 structure, are first attacked by water molecules and get protons from the decomposition of water molecules, resulting in the increase in pH value of solution. (2) Zinc ions react with water molecules and come off from the ZIF-8 structure. (3) Steps (1) and (2) are repeated until the chemical equilibrium is achieved, and the pH values and Zn^{2+} concentration become stable [78]. This results in ZIF-8 being used as a delivery system for osteogenic drugs in addition to its osteogenic properties [20]. This is because ZIF-8 has pH-responsive decomposition properties and exhibits stability in biologically relevant solutions, maintaining its crystal structure at pH 7.4 while being prone to degradation at pH 5.0 [79]. The pH-responsive dissolution trend occurs mainly because the acidic environment protonates methylimidazole (pKa ~ 7.35), which may decrease the coordination interactions and lead to a damaged network [80] (Fig. 4).

The above processes mainly occur under low pH conditions. However, due to the diversity of body fluid composition, ZIF-8 can also be degraded under physiological conditions through many different mechanisms. The study by Luzuriaga et al. [81] showed that neither phosphate nor carbonate-based buffers are harmless, even at pH above 7.4, and that exposure to these buffers causes changes in ZIF-8 morphology, as well as new and altered reflections in powder x-ray diffraction spectroscopy (PXRD) modes, almost immediately. Among them, potassium phosphate buffer (KP) completely eliminated ZIF-8 and replaced it with a completely different crystalline material. Energy dispersive x-ray (EDX) spectroscopy showed that the resulting constituent crystals were likely to be zinc and potassium phosphate, with very little MeIm remaining on the surface. However, even if ZIF-8 itself is replaced by phosphate, these buffers do not appear to cause cargo leakage in the ZIF-8 crystals. Similar findings were made by Velásquez-Hernández et al. and Taheri et al. on the degradation of ZIF-8 in buffers [82,83]. These findings elucidate the mechanism of the degradation process of ZIF-8 in phosphate solution, i.e., in solution, the coordination equilibrium between Zn^{2+} and MeIm is altered by the presence of phosphate species. This phosphate has a high affinity for Lewis metal centers, shifting the equilibrium towards the formation of insoluble inorganic by-products. Competition of phosphate species for metal centers progressively releases MeIm in solution. In fact, under these conditions, ligands are present in solution in the form of protonation species, which reduces the complexing capacity of the linker to cations. The decomposition kinetics depends on the size of the ZIF-8 particles, and the decomposition is faster for smaller particles [82].

In addition to buffers, the study by Luzuriaga et al. [81] found that serum proteins can solubilize ZIF-8, the effects of which are imperceptible to PXRD but can lead to leakage of cargo embedded in the crystal matrix. Spitsyna et al. [84] found that fetal bovine serum contributed negligibly to the dissolution of ZIF-8 nanoparticles at specific concentrations (10%) compared to other pathways. The study suggests that the degradation of nanoparticles can also be caused by the binding of zinc ions to amino acids, especially histidine and cysteine. This can be explained by the chemical properties of amino acids. For histidine, the zinc ion forms a six-membered chelating ring by coordinating with the two nitrogen atoms of the histidine moiety, which may be more stable than similar nitrogen atoms to other amino acids. In contrast, other amino acids form a five-membered chelating ring by coordinating with nitrogen and oxygen [85]. Therefore, their complexes with zinc ions are not as stable as histidine. The sulfur atom of cysteine has a high affinity for zinc ions, which results in cysteines also exhibiting high stability with zinc ion complexes, despite the five-membered chelating ring [86]. Thus, there are at least two contributions that lead to the instability of the ZIF-8: amino acids and buffer components. The main factors that play a different role in different solutions are different, mainly by reducing the concentration of Zn^{2+} and changing the degradation equilibrium. The reduction in the amount of free Zn^{2+} and the toxicity of newly formed zinc compounds in turn affect the overall toxicological effects of ZIF-8 in different media, so in order to successfully apply ZIF-8 in biomedical and environmental applications, it is important to have a clear understanding of how its chemical properties vary according to the physicochemical properties of the environment [83].

Due to the cytotoxicity of high concentrations of Zn^{2+}, the excessively fast release rate of Zn^{2+} from the material may harm bone tissue

Table 2
Results of in vivo studies.

Author/Year	Group/treatment	Animal	Sample size	Animal bone defect model	Post-Operative Observation Period	Bone regeneration measurement	Results	Other results
Zhang et al. 2017 [42]	Ti; AHT; ZIF-8@AHT-1/8	Female mice (2–3 months old)	18	A maxillary bone defect on the first molar sites	7 days	Movat's pentachrome staining, Aniline blue staining, picrosirius red staining, ALP activity, TRAP activity, Immunohistochemistry	Increased osseointegration at the bone-implant interface in the ZIF-8@AHT-1/8 group	
Liu et al. 2020 [46]	Control; Bone (treated with bone grafts); CA-CS&B; CA-CS/ZM&B	Male SD rats (8 weeks old)	24	A cranial bone defect of size approximately 5.5 mm in diameter	8 weeks	Micro CT, H&E staining, Masson trichrome staining, Sirius Red staining;	Largest new bone formation area and thickness in CA-CS/ZM&B group	Increased new blood vessels in CA-CS/ZM&B
Tao et al. 2020 [47]	Ti; Col I; MOF; MOF@Levo; MOF@Levo/LBL	SD rats (2 months old, 200–250 g)	50	A defect of approximately 10 mm in length and 1.5 mm in diameter on the distal end of the femur with *S. aureus* infection	4 weeks	H&E staining, Masson's trichrome staining, Giemsa staining, immunohistochemical staining, immunofluorescence staining	The highest percentage (37.6%) of new bone formation area in the MOF@Levo/LBL group, followed by MOF (33.7%), MOF@Levo (28.8%), native Ti (15.3%), and Col I (12.5%) groups	Decreased bacterial infection in MOF-modified groups
Zhong et al. 2020 [48]	Empty defect (control); PCL scaffold; PCL/DCPD scaffold; PCL/DCPD/nano ZIF-8 scaffold (0.5 wt% nano ZIF-8)	Male New Zealand rabbits (12 weeks old, 2.5 ± 0.2 kg)	24	A calvarial defect of 10 mm in diameter and 3 mm in thickness	12 weeks	Micro-CT, H&E staining, Masson's trichrome staining, immunohistochemistry	Increased calvarial defect healing in nano ZIF-8 incorporation group	
Fardjahromi et al. 2021 [50]	Empty defect (control); Osteon; ZIF8-Osteon	Male New Zealand rabbits (adult, 2.5–3.0 kg)	4	A calvarial defect of approximately 2 mm in depth and 8 mm in diameter	4 weeks	X-ray radiography, H&E staining,	Increased bone density in the ZIF8-Osteon-grafted defects	
Gao et al. 2021 [51]	SA hydrogel; SA/nano ZIF-8 hydrogel (50 μg mL^{-1}); Nothing SA/micro ZIF-8 (35 μg mL^{-1}, later supplementation)	Male SD rats (8 weeks old)	30	A bone defect with the size of 7*4*3 mm*3 on the maxillary central incisor to the first molar	4 or 8 weeks	Micro-CT, H&E staining, Masson trichrome staining, Sirius Red staining, immunohistochemical staining, immunofluorescence staining	Increased BV/TV ratio in the SA/nano ZIF-8 group; micro ZIF-8 also showed the capacity to induce osteogenic differentiation, but lower than nano ZIF-8	
Teng et al. 2021 [52]	TC4; MAO; MAO + Z; MAO + ZI	Male SD rats (8 weeks old)	12	A channel bone defect on the tibial tuberosity of 1 mm in diameter with an infection	4 and 8 weeks	Micro-CT, H&E staining, Masson trichrome staining	More contact bony tissue around the group of MAO, MAO + Z, and MAO + ZI, especially MAO + ZI	Decreased bacterial infection in MAO + Z and MAO + ZI groups, especially in the MAO + ZI group with NIR exposure
Toprak et al. 2021 [53]	Negative control group; PCL; PCL/ZIF-8; PCL/BMP-6@ZIF-8	Female Wistar rats (250–350 g)	24	A skull defect of 5 mm in diameter	8 weeks	Micro-CT, H&E staining, Masson's trichrome staining	PCL/ZIF-8 group and PCL/BMP-6@ZIF-8 group demonstrated better bone regeneration, especially in PCL/BMP-6@ZIF-8 group	
Xue et al. 2021 [54]	Blank; Col; PCL/Col; PCL/Col/ZIF-8 composite	Male SD rats (7 weeks old, 200 g)	20	A full-thickness cranium bone defect of 5 mm in diameter	8 weeks	Micro-CT, H&E staining, immunohistochemical staining	Bone-healing efficacy followed the trend of Blank < PCL/Col < Col < PCL/Col/ZIF-8 composite group	Remarkably better vascularization in the PCL/Col/ZIF-8 composite group
Al-Baadani, M et al. 2022 [55]	Control; PG; PG/ZIF-8(0.5%); PG/Aln; PG/Aln-ZIF-8 (0.5%)	SD rats		A cranial bone defect of 5 mm in diameter in the osteoporotic model after	4 and 8 weeks	Micro-CT	The bone regeneration capacity in PG/ZIF-8 (0.5%) and PG/Aln groups was significantly higher	

Table 2 (*continued*)

Author/Year	Group/treatment	Animal	Sample size	Animal bone defect model	Post-Operative Observation Period	Bone regeneration measurement	Results	Other results
				bilateral ovariectomy			than that of the control and PG groups, but PG/Aln-ZIF-8(0.5%) group showed the most augmented new bone formation	
Deng et al. 2022 [56]	sPEEK; pDA-sP; S@Z3-sP	Male SD rats (240 and 300 g)	24	A cylindrical bone defect matching the size of implanted materials	6 and 12 weeks	Micro-CT, fuchsin staining, immunofluorescence staining	Much denser bone coverage is observed on S@Z3-sP compared with others	ZIF-8 in combination with NIR has a good anti-infection effect
Liang et al. 2022 [58]	Control (the mixture of Matrigel (30 μL) and suspension in PBS without nanoparticles(20 μL)); ZIF-8 (25 μg mL^{-1}); DEX@ZIF-8 (25 μg mL^{-1}); DEX@ZIF-8-SCM (25 μg mL^{-1})	Wistar rats (6–8 weeks old)	20	A columnar defect of 2 mm in diameter and 8 mm in length along the longitudinal axis on the side face of the femur, approaching the knee joint	8 weeks	Micro-CT, H&E staining, immunofluorescence staining	The new bone volume ratio followed the trend of Control < ZIF-8 < DEX@ZIF-8 < DEX@ZIF-8-SCM	
Liu et al. 2022 [61]	Blank control group; Negative control group (periodontitis); GelMA; GelMA-ZH (0.2% *w/v*)	Male Wistar rats (6 weeks old)	24	A bone defect around the neck of the bilateral maxillary first molars with an inflammation	4 weeks	Micro-CT, H&E staining, Masson trichrome staining	Increased BV/TV ratio in the GelMA-ZH group	Reduced bacterial inflammation around periodontal tissue in the GelMA-ZH group
Ni et al. 2022 [62]	PLGA-TCP scaffold; ZIF-8-PDA@COL/PLGA-TCP scaffold; PDGF@ZIF-8-PDA@COL/PLGA-TCP scaffold	SD rats		A cranial bone defect of 5 mm in diameter	1 and 2 months	Micro-CT, Alizarin staining, tetracycline staining, calcein fluorochrome staining, H&E staining, Masson trichrome staining, AR staining, immunofluorescence staining	Increased bone regeneration efficacy in ZIF-8-PDA@COL/PLGA-TCP and PDGF@ZIF-8-PDA@COL/PLGA-TCP groups, especially in PDGF@ZIF-8-PDA@COL/PLGA-TCP group	
Qiao et al. 2022 [64]	Normal control; Hyperlipidemic control; PS (hyperlipidemia); nZPS (hyperlipidemia); nSZPS (hyperlipidemic)	Male SD rats (6 weeks old)	60	A skull bone defect of 4 mm in diameter; A premaxillary bone defect with the size of 7*4*3 mm*3	8 weeks	Micro-CT, H&E staining, Masson trichrome staining and Sirius Red staining, immunofluorescence staining	Increased bone recovery in nZPS and nSZPS groups, especially in the nSZPS group	
Ren et al. 2022 [65]	Control; ZIF-8 (25 μg mL^{-1}); SCM/ZIF-8 (25 μg mL^{-1})	Wistar rats (6–8 weeks old)	15	A femoral bone defect of 2 mm in diameter and 8 mm in length along the longitudinal axis	4 weeks	Micro-CT, H&E staining, Masson staining	Increased bone recovery in ZIF-8 and SCM/ZIF-8 groups, especially in SCM/ZIF-8 group	
Shi et al. 2022 [66]	Control; Z10-FG (10 μg mL^{-1}); Z20-FG (10 μg mL^{-1})	SD rats (12 weeks old)	18	A cranial bone defect of 8 mm in diameter	12 weeks	Micro-CT, H&E staining, Masson's trichrome staining, immuno-histochemistry analysis	Increased new bone volume in Z10-FG and Z20-FG groups, especially in the Z20-FG group	
Wang et al. 2022 [67]	Ti; TNT; TNT-ZIF-8; TNT-ZIF-8@Nar	Male SD rats (8 weeks old, 220–250 g)	40	A cylindrical defect of 1.5 mm in diameter between the diaphysis and epiphysis of the femur	4 weeks	H&E staining, Masson's trichrome staining	Increased bone regeneration in TNT-ZIF-8@Nar and the TNT-ZIF-8 groups, especially in the TNT-ZIF-8@Nar group	Decreased bacterial viabilities in MOF-modified groups

Table 2 (*continued*)

Author/Year	Group/treatment	Animal	Sample size	Animal bone defect model	Post-Operative Observation Period	Bone regeneration measurement	Results	Other results
Zhang et al. 2022 [69]	SA hydrogel (control); ZIF-8 hydrogel; OD@ZIF-8 hydrogel	Male SD rats (6 weeks old, 180 g)	9	A cranial bone defect of 5 mm in diameter	4 weeks	Micro-CT, H&E staining, Masson's trichrome staining, Sirius red staining, immunofluorescence staining	Increased bone regeneration in OD@ZIF-8 and ZIF-8 groups, especially in OD@ZIF-8 group	Increased the secretion of angiogenesis-related proteins in the DMOG@ZIF-8 group
Hu et al. 2023 [71]	Control; Bio-Oss; L-DP-Bio-Oss; L-DPZ2-Bio-Oss	New Zealand rabbits (female, 10–12 weeks old, 2.5–3 kg)		A cranial bone defect of 10 mm in diameter	4 or 8 weeks	Micro CT, Van Gieson's (VG) picrofuchsin staining	The bone defects treated with the combination of Bio-Oss granules and the LDPZ2 hydrogel exhibited the best osteogenesis outcome	
Lao et al. 2023 [72]	Blank (control); Blank (Diabetes); GelMA (Diabetes); GelMA/Metformin (Diabetes); GelMA/ZIF-8 (Diabetes); GelMA/Met@ZIF-8(Diabetes)	SD rats		Two full-thickness bone defects of 5 mm diameters on the two sides of rats' calvaria region	10 weeks	Micro-CT, H&E staining, Masson staining, immunofluorescence	Suppressed bone defect regeneration in the diabetic condition(the bone volume/total volume was 5.3% ± 4.3%) whereas GelMA/Met@ZIF-8 changed the suppression and promoted bone regeneration(39.7% ± 2.3%)	
Li et al. 2023 [74]	SA hydrogel; SA/DFO; SA/ZIF-8; SA/DFO@ZIF-8	SD rats (male, 7 weeks old, 200 g)	48	A cranial bone defect of 5 mm in diameter	4 week	Micro-CT, H&E staining, Masson trichrome staining, Sirius Red staining, Immunohistochemical, and Immunofluorescence Analyses	The increased trend is SA hydrogel < SA/DFO < SA/ZIF-8 < SA/DFO@ZIF-8	The promoted formation of a vascular network trend is SA hydrogel < SA/ZIF-8 < SA/DFO < SA/DFO@ZIF-8

regeneration by affecting the proliferation and differentiation of osteoblasts [23]; the rate of degradation being too fast also is not conducive to the long-term role of ZIF-8 and its loaded drugs [48]. In addition, ZIF-8 particles are usually unfixable at bone-defect sites. Therefore, ZIF-8 typically must be implanted with other materials or modified for further use. For example, it can be used as a coating on implant surfaces after polydopamine modification [49] or encapsulated in materials such as hydrogels [61], stem cell membranes [65], or electrospun scaffolds [40]. These methods are essential for protecting ZIF-8 from direct exposure to body fluids, protecting the loaded drug, and achieving sustained release of active ingredients. Simultaneously, the partially loaded drug itself can interact with ZIF-8 [87]. For example, when loaded with dexamethasone, the drug stabilizes the ZIF-8 structure and inhibits the release of Zn^{2+} [28]. Al-Baadani et al. [55] showed that alendronate has a similar stabilization effect.

ZIF-8 materials sometimes exhibit early burst release rates. This may be due to the fact that the dissolution of ZIF-8 structure in aqueous solution can be considered as a reverse synthesis process, and the 2-methylimidazole produced by the dissolution has an inhibitory effect on the degradation of the ZIF-8 layer [78]. Chen et al. fabricated a polydopamine-coated ZIF-8 coating on sPEEK, which facilitated the controlled release of Zn^{2+}. Z-1/sPEEK and Z-3/sPEEK exhibit burst release for the first 48 h and then continue to release slowly, with total Zn^{2+} releases at 144 h approximately 0.07 and 0.154 μg mL^{-1}, respectively [49]; these concentrations are lower than previously reported potentially cytotoxic-inducing concentrations of Zn^{2+} [88]. The rapid release of Zn^{2+} over a short period likely originates from the collapse of the ZIF-8 nanoparticles exposed on the coating surface. Because the short-term burst release of Zn^{2+} has an adverse effect on initial cell attachment, the density of adherent cells on the modified surface is lower than that on pure sPEEK. However, it is also believed that early

burst release is beneficial in the clinical environment because it is likely to cause local Zn^{2+} ions to reach an effective threshold within a short period, thereby triggering osteoblast stem cell recruitment and coordinating the subsequent osteogenic differentiation process [54].

4.2. Biocompatibility of ZIF-8 materials

Before the use of ZIF-8 as an osteogenic material, its biocompatibility with osteoblast-related cells must be verified. Biocompatibility is one of the main factors considered in materials for biomedical applications [89] and can be defined as the ability of a material to perform its programmed functions (e.g., delivering drugs in the human body) without adversely affecting the surrounding tissues or altering homeostasis [90].

ZIF-8 contains divalent zinc ions (Zn^{2+}) and 2-methylimidazole (MeIm). The skeleton structure of ZIF-8 is relatively stable under normal physiological conditions; however, under acidic conditions, degradation accelerates owing to the protonation of organic ligands in the framework [91], releasing Zn^{2+} and 2-methylimidazole. 2-Methylimidazole has been thoroughly studied and found to have no significant toxicological effects in in vivo studies in rats [92]. It must be noted that MeIm is classified as a mild carcinogen by the International Agency for Research on Cancer (IARC) even though its carcinogenicity was only observed at very high doses (>5000 ppm) [93]. However, increased intracellular Zn^{2+} concentrations have been shown to inhibit the tricarboxylic acid cycle associated with enzymes such as glycerol-3-phosphate dehydrogenase, induce permeability shifts in mitochondrial membranes, and inhibit mitochondrial bc$_1$ cytochrome complexes, leading to increased production and accumulation of reactive oxygen species (ROS) [94–97]. ROS species are well-known genotoxic substances that cause DNA damage by oxidizing DNA base pairs [98,99]. If ROS levels are above a certain threshold, DNA repair is no longer
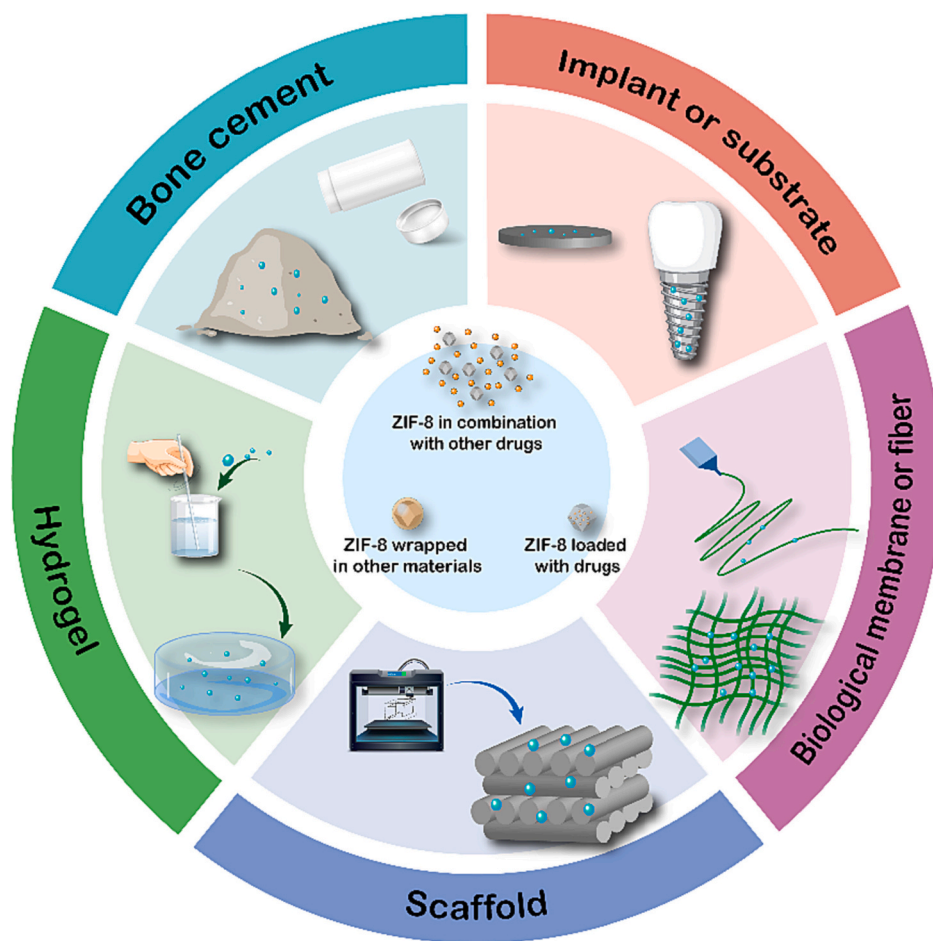
Fig. 3. Schematic illustration of composite material introduced with ZIF-8 particles.
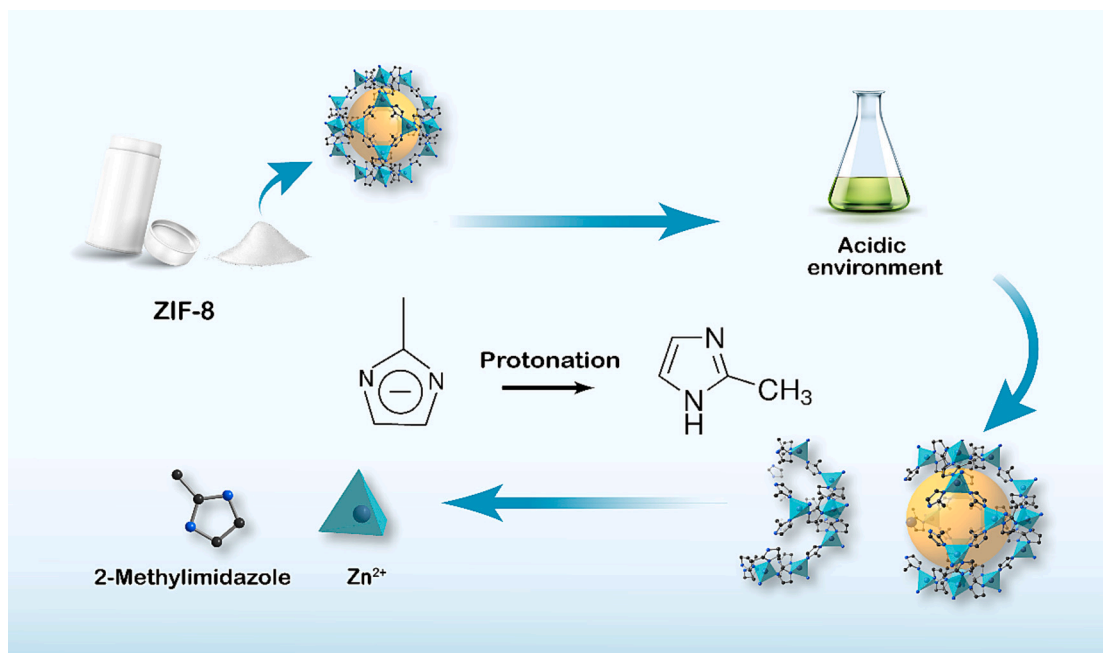

Fig. 4. Schematic diagram of ZIF-8 decomposition under acidic conditions. Under acidic conditions, 2-methylimidazole (pKa ~ 7.35) protonation and ZIF-8 network decomposition release Zn^{2+} and 2-methylimidazole.

possible, eventually inducing an apoptosis pathway [100]. Although Zn^{2+} stored in ZIF-8 can be released at a relatively slow rate as ZIF-8 decomposes, as the concentration of ZIF-8 increases, the concentration of Zn^{2+} increases and the production of ROS increases, resulting in apoptosis. Previous studies have found that ZIF-8 exhibits significantly reduced biocompatibility above a specific particle concentration of 30 $\mu g \, mL^{-1}$ or Zn^{2+} concentration above 4 $\mu g \, mL^{-1}$ [101]. Therefore, ZIF-8 must be present at an optimal concentration to express its bone-regeneration-promoting properties.

Of the 39 papers under discussion, 16 investigated the biocompatibility of different concentrations of ZIF-8 in vitro for various cells, and 12 in vitro studies showed dose-dependent ZIF-8 cytotoxicity. However, the threshold for the cytotoxicity of ZIF-8 differs among different cells. For rBMSCs, nano ZIF-8 shows the highest activity in cells at a concentration of 50 $\mu g \, mL^{-1}$; above this value, it exhibits pro-apoptotic properties [44,51]. For HUVEC, this value is 75 $\mu g \, mL^{-1}$ [44]. Ge et al. found that the results obtained using MC3T3-E1 cells indicate greater tolerance than the results of other researchers, and the number of cells cultured decreases dramatically when ZIF-8 concentrations exceed 200 $\mu g \, mL^{-1}$ [57]. Shi et al. found that EMSCs has a higher sensitivity to ZIF-8, which has anti-apoptotic properties at concentrations <20 $\mu g \, mL^{-1}$ and pro-apoptotic effects at concentrations >30 $\mu g \, mL^{-1}$ [66].

In addition to its concentration, the biocompatibility of ZIF-8 is affected by the size of ZIF-8. This is mainly due to the effect of the Zn^{2+} concentration produced by degradation. In all studies discussing the size of ZIF-8, this size was almost always in the nanometer range, and only Chen et al. [41] studied the biocompatibility of ZIF-8 at different particle sizes. The biodegradation results showed that the amount of zinc produced by the nano ZIF-8 (200–300 nm) film remained almost unchanged after four days, and the zinc ion concentration peaked at 7.36 $\mu g \, mL^{-1}$ at 14 days. In contrast, the micro ZIF-8 (10 μm) film showed a higher Zn ion concentration of up to 30.91 $\mu g \, mL^{-1}$ on the first day, which increased to 57.23 $\mu g \, mL^{-1}$ on the 14th day. Thus, it was confirmed that nano ZIF-8 has good biocompatibility whereas micro ZIF-8 has evident cytotoxicity to MG63 cells. However, differences in zinc ion concentrations may also be related to the discrete distribution of nano ZIF-8 on the porous titanium surfaces, as uncovered spaces and exposed titanium surfaces may reduce the zinc composition of the nano ZIF-8 films [41]. At this release concentration, the nano ZIF-8 membrane can not only enhance the ALP activity of MG63 cells, upregulate osteogenic genes, and promote extracellular matrix (ECM) mineralization, but also inhibit the growth of *Streptococcus mutans*.

Regarding the toxicity study in mammals, Li et al. [91] injected ZIF-8 nanoparticles into mice with a dose of 32 $mg \, kg^{-1}$ intravenously for a total of 4 times, and after 1 day, there was a large number of particles in the capillaries of the lungs, and the lungs and kidneys were slightly damaged, but over time, the drug level decreased dramatically, and on the 7th day after the 4 intravenous injections, the removal rate exceeded 70%, and the degree of lung and kidney lesions also improved. This means that ZIF-8 has a good clearance rate in vivo. Of the animal studies included in the review, seven studies reported toxicological results of ZIF-8 in rats without drug loading [47,51,54,61,64,71,74], with no significant toxicity or injury detected by relevant hematological and organ histology. These toxicity experiments proved that ZIF-8 has good biological safety. For better fixation, ZIF-8 is usually implanted in the body with implants such as hydrogel or titanium rods, including bone defects in the femur, jaw, or skull. An implantation concentration of 100 $\mu g \, mL^{-1}$ in sodium alginate (SA) hydrogel has been reported [51], while Liu et al. [61] injected ZIF-8 particles doped into gelatin methacryloyl (GelMA) hydrogel into periodontal pockets at a concentration of 2 mg mL^{-1}. Qiao et al. [64] and Hu et al. [71] performed toxicological tests by implanting the material under the skin alone. It should be noted that these subsequent animal experiments were based on previous cell experiments, the more daring high doses were not adopted, and the application of other implants also delayed the release of ZIF-8.

Therefore, there is a need to further explore the safe dose of ZIF-8 for topical use in vivo. For example, in the study of Kumar et al. [102], ZIF-8 in the injection range of 50–1000 μg was administered intranasally to female mice with no toxicological effect. But this is different from the application scenario of bone regeneration.

### 4.3. Osteogenesis induction ability of ZIF-8 material and its mechanism

ZIF-8 can affect the osteogenic differentiation ability of cells, which may be due to various effects. ZIF-8 exhibits pH-responsive decomposition properties [79]. The release of Zn^{2+} can affect osteoblast-related activities and promote osteoblast diffusion [103], attachment [104], and chemotaxis [105]. Nano-sized ZIF-8 can also enter cells through endocytosis to promote osteogenesis [51].

Cellular and molecular evidence suggests that the incorporation of Zn^{2+} into biomaterials can upregulate the expression of osteocyte-associated genes, such as ALP, runt-related transcription factor 2 (Runx2), collagen type I (Col I), osteopontin (OPN), and osteocalcin (OCN) [106–111]. Zn^{2+} can enter the cell through TRPM7 and GPR39 receptors, and Zn^{2+} entering the cell activates the cAMP-PKA pathway and the parallel Gαq-PLC-IP3 pathway. Both may lead to intracellular Ca^{2+} responses and the activation of downstream MAPK/ERK and AKT pathways, mainly the ERK pathway, which leads to the osteogenic differentiation of human bone marrow mesenchymal stem cells (hBMSCs) [51,112]. It has also been reported that Zn^{2+} entering cells can activate Runx2 through the cAMP-PKA-CREB signaling pathway, thereby inducing osteogenesis in hBMSCs [113]. In addition, Cho and Kwun found that zinc induces Runx2 expression increase through the typical BMP-2/Smad-1 signaling pathway in MC3T3-E1 (subclone 4) cells. [114]

Runx2 is a specific transcription factor involved in osteogenic differentiation and is the earliest and most specific marker gene involved in bone formation [114]. Runx2 also upregulates the expression of several specific markers related to osteoblast proliferation and differentiation, such as ALP, OCN, and OPN [115]. OPN is an important glycosylated bone matrix protein that is widely distributed in the extracellular matrix and mediates osteoblast adhesion, migration, and proliferation [116]. OCN is a calcium-binding protein synthesized by differentiated mature osteoblasts, is deposited primarily in the bone matrix, and is one of the hallmarks of osteoblast mineralization [117]. ALP is a Zn^{2+} metallized glycoprotein that can be used to reflect early osteogenic differentiation [118]. As a natural cation in ALP, Zn^{2+} has been shown to promote its stability and activity [119]. Due to the characteristics of these osteogenic markers, the 39 papers included in the statistics examined and analyzed many or all of the above markers.

The release of Zn^{2+} from loaded ZIF-8 particles creates a local alkaline microenvironment [120], which can improve the secretion of type I collagen and the activity of ALP, as well as increase the expression level of osteogenesis-related genes [60]. Previous studies have shown that a weakly alkaline environment (pH = 7.4) can increase HAp accumulation [121]. At the same time, the osteolytic activity of osteoclasts is significantly weakened under alkaline conditions, resulting in more calcium mineralization deposits, which are conducive to the nucleation and growth of HAp [122,123].

The effect of Zn^{2+} on ALP activity and other osteogenic processes shows a biphasic dose response, with positive effects on osteoblast activity occurring in a narrow dose range of 1–50 μM; doses above this range inhibit osteogenic activity, and doses below this range have no measurable effect [124]. Therefore, for ZIF-8, there is an optimal stimulation concentration. Of the 39 studies under discussion, seven in vitro experiments investigated the ability of different levels of ZIF-8 to promote osteogenesis. Among them, Gao et al. reported that nano ZIF-8 at 50 $\mu g \, mL^{-1}$ is the optimal stimulus concentration for osteogenic differentiation of rBMSCs relative to other concentrations [51]. Shi et al. also reported that 20 $\mu g \, mL^{-1}$ of nano ZIF-8 has the best stimulation effect on the osteogenic differentiation of EMSCs [66]. These results are
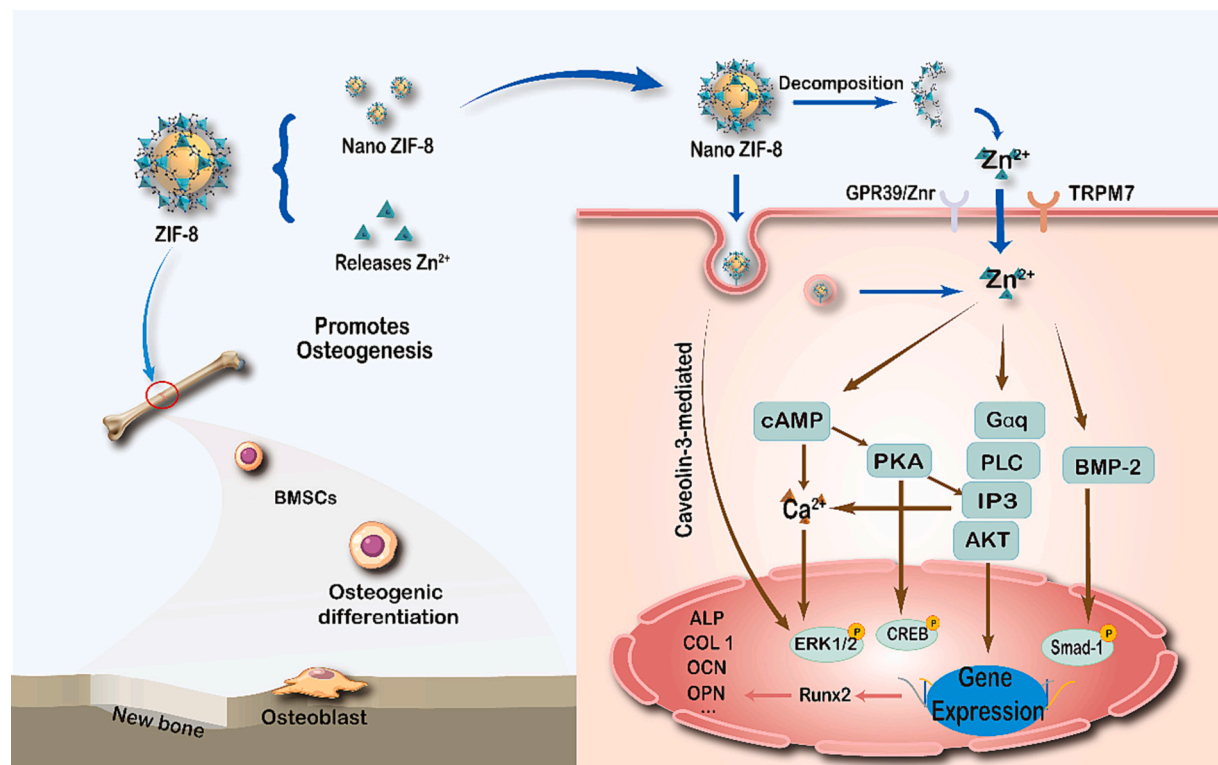
Fig. 5. Schematic illustration of osteoblast differentiation promotion mechanism of ZIF-8. ZIF-8 promotes osteogenesis through nanoforms or by releasing Zn^{2+}. Nano ZIF-8 can be internalized by BMSCs via CvME and macropinocytosis, releasing Zn^{2+} within cells or after decomposition in vitro. The resulting Zn^{2+} enters the cell through the TRPM7 and GPR39 receptors. Then, Zn^{2+} entering the cell activates the cAMP-PKA pathway and the parallel Gαq-PLC-IP3 pathway and triggers the intracellular Ca^{2+} response, leading to the canonical MAPK/ERK and AKT pathways activation, mainly the ERK pathway; Zn^{2+} entering cells can also activate Runx2 through the cAMP-PKA-CREB signaling pathway or the typical BMP-2/Smad-1 signaling pathway; During the entry of nano ZIF-8 into cells, CvME internalization may trigger Caveolin-3-mediated MAPK activation. All these signaling pathways lead to related gene expression and osteogenic differentiation of BMSC.

consistent with the concentration results for ZIF-8 biocompatibility.

In addition to releasing Zn^{2+} outside the cell, nano-sized ZIF-8 itself can also enter the cell through endocytosis to promote osteogenesis, similar to the uptake of exosomes [51]; this feature is used to deliver drugs with a poor ability to penetrate membranes, such as MicroRNAs [35]. Gao et al. stated that this may be the main method for nano ZIF-8 to enter cells to play a bone-promoting role [51]. Nano ZIF-8 can be internalized by rBMSCs via CvME and macropinocytosis, releasing Zn^{2+} within the cells. Previous studies have reported that extracellular Zn^{2+} is transferred into the cells and activates the cAMP-PKA pathway, which triggers a Ca^{2+} response in the cytoplasm, thereby activating the MAPK pathway [112]. Zn^{2+} produced by nano ZIF-8 entering the cells also activates the MAPK pathway at the same time. During the entry of nano ZIF-8 into rBMSCs, CvME internalization may also trigger Caveolin-3-mediated MAPK pathway activation, thereby promoting osteogenesis (Fig. 5); however, the exact interaction between nano ZIF-8 and possible cell membrane receptors is yet to be elucidated [51]. In addition to the aforementioned pathways, the transcriptional process may also be altered if loaded with drugs. For example, Liang et al. found that ZIF-8 loaded with dexamethasone mainly promotes bone regeneration by activating the phosphoinositide 3-kinase (PI3K)-Akt signaling pathway [58].

Other possible mechanisms have also been proposed. For example, nano-sized ZIF-8 can form a nanoscale morphology on the surface of implantation materials and increase cell attachment [125]. The degradation of ZIF-8 crystals exposes the nucleation site on the substrate surface, the surface of the degraded ZIF-8 crystals, and the junction zone of the two, thereby enhancing the nucleation of calcium and the formation of hydroxyapatite crystals and synergizing with the ZIF-8

crystals themselves to improve osteogenic activity [41].

The characteristics of large specific surface area, high pore volume, and uniform pore size and pore distribution make ZIF-8 an excellent drug carrier [25] that can perform a variety of functions by loading multiple types of drugs to cope with a variety of problems that need to be solved in the process of bone defects. Of the 39 studies analyzed, 25 used ZIF-8 in combination with other drugs. To analyze the role of ZIF-8 in composite materials, we required that all included studies have a reasonable experimental group design. Therefore, the studies included in the statistical analysis had corresponding control groups to compare the effects of adding or lacking ZIF-8 on the osteogenic properties of the materials.

All 25 papers included reported that the addition of ZIF-8 improves the osteogenesis-related parameters of the composites compared to a single material or drug alone. However, five papers [39,43,47,58,67] reported that in the experimental group with only ZIF-8, the difference in osteogenesis-related parameters between the ZIF-8 group and the control group was not significant, while in two studies [53,77], some osteogenesis-related parameters in the experimental group with only ZIF-8 were lower than those in the control group, which may be due to the failure to select the appropriate ZIF-8 content. Follow-up animal studies were conducted in four of the seven in vitro studies [47,53,58,67]. In these four animal studies, the osteogenic capacity of the ZIF-8 group was superior to that of the control group, which differed from the results of the corresponding in vitro studies. This may be because the local concentrations of ZIF-8 or Zn^{2+} are different from those in vitro owing to the dynamic changes in in vivo environments [126]. Therefore, the search for optimal, safe and osteogenic concentrations of ZIF-8 should not be limited to in vitro studies.
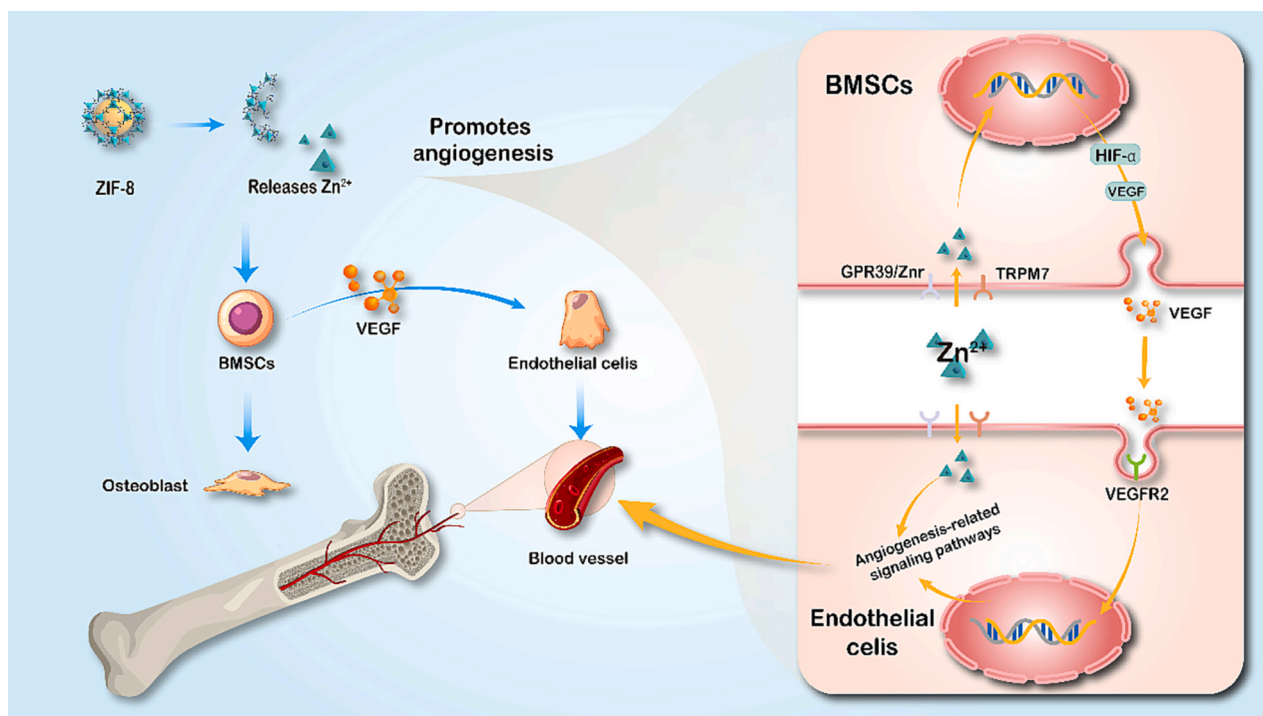
Fig. 6. Schematic illustration of nano ZIF-8 promoting vascularization osteogenesis.

4.4. Angiogenesis induction ability of ZIF-8 and its mechanism

Traditional bone repair strategies focus on the formation of new bone, and early vascularization of new bone is important during bone formation. The growth of blood vessels that supply nutrients and remove metabolites always precedes osteogenesis and is critical for continuous skeletal development [127–129]. Therefore, angiogenesis is essential for successful bone regeneration, particularly in large-sized bone defects.

Five articles [44,46,54,69,74] investigated the angiogenic effects of ZIF-8 materials, and ZIF-8 shows good vasogenic activity at appropriate doses; ZIF-8 promotes angiogenesis via an indirect effect [46]. Zn^{2+} can upregulate the production of VEGF-A in osteoblasts [130], and vascular endothelial growth factor (VEGF) is an important regulator of angiogenesis with high specificity for vascular endothelial cells; its continuous secretion may promote angiogenic activity around endothelial cells [131]. The VEGF family includes VEGF-A, VEGF-B, VEGF-C, VEGF-D, the virus-encoded VEGF-E, the snake venom-derived VEGF-F and Placental Growth Factor (PlGF) [132]. VEGF-A is the best characterized family member being the most potent stimulator of angiogenic processes, able to bind to receptors on the endothelium and stimulate proliferation and cell migration [133]. The angiogenic response to VEGF-A in vivo is achieved by activating the vascular endothelial growth factor receptor 2 (VEGFR2) [134]. VEGFR2 activation can lead to vascular permeability through FAK recruitment [135,136], p38 MAPK-mediated actin cytoskeletal reorganization [137] and eNOS activation [138,139], and can also lead to proliferation via ERK1/2 [140] and PLCγ [141], adhesion kinase (FAK)-mediated cell migration [142], and cell survival through phosphatidylinositol-4,5-bisphosphate 3-kinase (PI3K)/protein kinase B (AKT) [143]. These downstream pathways intersect to promote the formation of blood vessels. In the corresponding in vitro experiments [54,69], the expression of VEGF was significantly increased, suggesting that ZIF-8 may stimulate its release from osteoblasts and contribute to the creation of a biochemical microenvironment that promotes angiogenesis [54].

However, the specific mechanism by which Zn^{2+} stimulate osteoblasts to produce VEGF has not been clearly reported. In the study of Li et al. [134], Zn^{2+} can significantly increase the levels of HIF-1α, VEGF-

A, VEGF-R2 proteins in astrocytes, and promote angiogenesis by regulating the astrocytes HIF-α/VEGF pathway. Hypoxia-inducible factor 1α (HIF-1α) plays an important protective role in promoting cellular adaptation to hypoxic conditions, is a major hypoxia response signaling protein that regulates angiogenesis, and participates in angiogenesis by stimulating VEGF [134]. In the experiment of Chen et al., the addition of Zn^{2+} significantly increased the expression of HIF-1α and VEGF in vivo [144]. Thus, the same mechanism of VEGF expression may exist in osteoblasts. In addition to the indirect effects of osteoblasts, in the report of Zhu et al., Zn^{2+} can directly promote vascular cell viability and proliferation through GPR39/Znr [145]. Therefore, the mechanism of Zn^{2+} and ZIF-8 promoting vascular regeneration in bone defect repair still needs further study.

At the same time, it should be noted that according to Liu et al., although all doses of ZIF-8 showed a good pro-angiogenic effect in vitro, the CA-CS/ZM groups (catechol−chitosan/ZIF-8 = 25:1 *w/w*) showed better angiogenic effects than the other groups, indicating that an appropriate dose of ZIF-8 can maximize the paracrine function of rBMSCs [46]. In subsequent animal experiments, more new blood vessels and fewer inflammatory cells were identified in the CA-CS/ZM group. (Fig. 6).

The zinc ions produced by ZIF-8 stimulate BMSCs to secrete VEGF, promote endothelial cells to form blood vessels, provide nutrients, and remove metabolites. BMSCs are stimulated by ZIF-8 to differentiate into osteoblasts to exert osteogenic function.

5. Conclusion

As a pH-responsive material, ZIF-8 can release Zn^{2+} when required, thereby avoiding cytotoxicity at high Zn^{2+} concentrations. Existing studies have shown that nano-sized ZIF-8 has good biocompatibility and is effective in bone regeneration and angiogenesis at concentrations below 100 μg mL^{-1}, and its promotion of osteoblast differentiation is mainly achieved by releasing Zn^{2+} inside and outside the cell to activate the canonical MAPK pathway. Moreover, its porous structural characteristics can be used for the delivery of other drugs, exerting multiple effects, and coping with various problems in the process of bone

regeneration. In conclusion, ZIF-8 exhibits different favorable properties and can be used in various bone tissue engineering applications.

CRediT authorship contribution statement

Hao Tang: Writing – original draft, Visualization, Project administration, Methodology, Investigation, Formal analysis, Data curation. **Yameng Yu:** Methodology, Data curation. **Xinxin Zhan:** Visualization, Methodology, Data curation. **Yuan Chai:** Methodology. **Yufeng Zheng:** Conceptualization. **Yunsong Liu:** Writing – review & editing, Supervision, Conceptualization. **Dandan Xia:** Writing – review & editing, Supervision, Resources, Methodology, Funding acquisition, Conceptualization. **Hong Lin:** Writing – review & editing, Supervision, Resources, Funding acquisition, Conceptualization.

Declaration of Competing Interest

The authors declare no conflict of interest.

Data availability

No data was used for the research described in the article.

Acknowledgements

Appendix A. Supplementary data

Supplementary data to this article can be found online at https://doi.org/10.1016/j.jconrel.2023.11.049.

References

[1] G.P. Chaves Filho, M. Lima, H.A.O. Rocha, S.M.G. Moreira, Role of sulfated polysaccharides from seaweeds in bone regeneration: a systematic review, Carbohydr. Polym. 284 (2022), 119204.

[2] R. Dimitriou, E. Tsiridis, P.V. Giannoudis, Current concepts of molecular aspects of bone healing, Injury 36 (12) (2005) 1392–1404.

[3] P. Grabowski, Physiology of bone, Endocr. Dev. 28 (2015) 33–55.

[4] S.H.S. Tan, J.R.Y. Wong, S.J.Y. Sim, C.K.E. Tjio, K.L. Wong, J.R.J. Chew, J.H. P. Hui, W.S. Toh, Mesenchymal stem cell exosomes in bone regenerative strategies-a systematic review of preclinical studies, Mater Today Bio 7 (2020), 100067.

[5] F. Re, E. Gabusi, C. Manferdini, D. Russo, G. Lisignoli, Bone regeneration improves with mesenchymal stem cell derived extracellular vesicles (EVs) combined with scaffolds: A systematic review, Biology (Basel) 10 (7) (2021), https://doi.org/10.3390/biology10070579.

[6] A.S. Greenwald, S.D. Boden, V.M. Goldberg, Y. Khan, C.T. Laurencin, R.N. Rosier, I. American Academy of Orthopaedic Surgeons, The Committee on Biological, Bone-graft substitutes: facts, fictions, and applications, J Bone Joint Surg Am 83-A Suppl 2 Pt 2 (2001) 98–103.

[7] P. Baldwin, D.J. Li, D.A. Auston, H.S. Mir, R.S. Yoon, K.J. Koval, Autograft, allograft, and bone graft substitutes: clinical evidence and indications for use in the setting of Orthopaedic trauma surgery, J. Orthop. Trauma 33 (4) (2019) 203–213.

[8] C.G. Finkemeier, Bone-grafting and bone-graft substitutes, J. Bone Joint Surg. Am. 84 (3) (2002) 454–464.

[9] H.S. Sohn, J.K. Oh, Review of bone graft and bone substitutes with an emphasis on fracture surgeries, Biomater Res 23 (2019) 9.

[10] J. Lee, H. Byun, S.K. Madhurakkat Perikamana, S. Lee, H. Shin, Current advances in immunomodulatory biomaterials for bone regeneration, Adv. Healthc. Mater. 8 (4) (2019), e1801106.

[11] A. Bharadwaz, A.C. Jayasuriya, Recent trends in the application of widely used natural and synthetic polymer nanocomposites in bone tissue regeneration, Mater. Sci. Eng. C Mater. Biol. Appl. 110 (2020), 110698.

[12] K. Qiao, L. Xu, J. Tang, Q. Wang, K.S. Lim, G. Hooper, T.B.F. Woodfield, G. Liu, K. Tian, W. Zhang, X. Cui, The advances in nanomedicine for bone and cartilage repair, J Nanobiotechnol. 20 (1) (2022) 141.

[13] M. Edelmayer, C. Wehner, C. Ulm, W. Zechner, D. Shafer, H. Agis, Which substances loaded onto collagen scaffolds influence oral tissue regeneration?-an overview of the last 15 years, Clin. Oral Investig. 24 (10) (2020) 3363–3394.

[14] X. Yan, P. Li, X. Song, J. Li, B. Ren, S. Gao, R. Cao, Recent progress in the removal of mercury ions from water based MOFs materials, Coord. Chem. Rev. 443 (2021), 214034.

[15] M. Li, S. Yin, M. Lin, X. Chen, Y. Pan, Y. Peng, J. Sun, A. Kumar, J. Liu, Current status and prospects of metal-organic frameworks for bone therapy and bone repair, J. Mater. Chem. B 10 (27) (2022) 5105–5128.

[16] W. Sun, S. Li, G. Tang, Y. Luo, S. Ma, S. Sun, J. Ren, Y. Gong, C. Xie, Recent Progress of nanoscale metal-organic frameworks in Cancer Theranostics and the challenges of their clinical application, Int. J. Nanomedicine 14 (2019) 10195–10207.

[17] B. Zou, Z. Xiong, L. He, T. Chen, Reversing breast cancer bone metastasis by metal organic framework-capped nanotherapeutics via suppressing osteoclastogenesis, Biomaterials 285 (2022), 121549.

[18] V.R. Cherkasov, E.N. Mochalova, A.V. Babenyshev, J.M. Rozenberg, I.L. Sokolov, M.P. Nikitin, Antibody-directed metal-organic framework nanoparticles for targeted drug delivery, Acta Biomater. 103 (2020) 223–236.

[19] Y. Han, F. Wang, J. Zhang, Design and syntheses of hybrid zeolitic imidazolate frameworks, Coord. Chem. Rev. 471 (2022), 214759.

[20] V. Hoseinpour, Z. Shariatinia, Applications of zeolitic imidazolate framework-8 (ZIF-8) in bone tissue engineering: a review, Tissue Cell 72 (2021), 101588.

[21] A.J. Zaitouna, R.Y. Lai, Design and characterization of a metal ion-imidazole self-assembled monolayer for reversible immobilization of histidine-tagged peptides, Chem. Commun. (Camb.) 47 (45) (2011) 12391–12393.

[22] W. Miao, J. Wang, J. Liu, Y. Zhang, Self-cleaning and antibacterial Zeolitic Imidazolate framework coatings, Adv. Mater. Interfaces 5 (14) (2018) 1800167.

[23] B. Jia, H. Yang, Z. Zhang, X. Qu, X. Jia, Q. Wu, Y. Han, Y. Zheng, K. Dai, Biodegradable Zn-Sr alloy for bone regeneration in rat femoral condyle defect model: in vitro and in vivo studies, Bioact Mater 6 (6) (2021) 1588–1604.

[24] M. Watroba, W. Bednarczyk, P.K. Szewczyk, J. Kawalko, K. Mech, A. Grunewald, I. Unalan, N. Taccardi, G. Boelter, M. Banzhaf, C. Hain, P. Bala, A.R. Boccaccini, In vitro cytocompatibility and antibacterial studies on biodegradable Zn alloys supplemented by a critical assessment of direct contact cytotoxicity assay, J Biomed Mater Res B Appl Biomater (2022), https://doi.org/10.1002/jbm.b.35147.

[25] H. Kaur, G.C. Mohanta, V. Gupta, D. Kukkar, S. Tyagi, Synthesis and characterization of ZIF-8 nanoparticles for controlled release of 6-mercaptopurine drug, J. Drug Deliv. Sci. Technol. 41 (2017) 106–112.

[26] M.J. Page, J.E. McKenzie, P.M. Bossuyt, I. Boutron, T.C. Hoffmann, C.D. Mulrow, L. Shamseer, J.M. Tetzlaff, E.A. Akl, S.E. Brennan, R. Chou, J. Glanville, J. M. Grimshaw, A. Hrobjartsson, M.M. Lalu, T. Li, E.W. Loder, E. Mayo-Wilson, S. McDonald, L.A. McGuinness, L.A. Stewart, J. Thomas, A.C. Tricco, V.A. Welch, P. Whiting, D. Moher, The PRISMA 2020 statement: an updated guideline for reporting systematic reviews, BMJ 372 (2021), n71.

[27] M.A. Khalili, E. Tamjid, Controlled biodegradation of magnesium alloy in physiological environment by metal organic framework nanocomposite coatings, Sci. Rep. 11 (1) (2021) 8645.

[28] N. Li, L. Xie, Y. Wu, Y. Wu, Y. Liu, Y. Gao, J. Yang, X. Zhang, L. Jiang, Dexamethasone-loaded zeolitic imidazolate frameworks nanocomposite hydrogel with antibacterial and anti-inflammatory effects for periodontitis treatment, Mater Today Bio 16 (2022), 100360.

[29] S.A. Salim, A.A. Taha, E.E. Khozemy, S.H. El-Moslamy, E.A. Kamoun, Electrospun zinc-based metal organic framework loaded-PVA/chitosan/hyaluronic acid interfaces in antimicrobial composite nanofibers scaffold for bone regeneration applications, J. Drug Deliv. Sci. Technol. 76 (2022), 103823.

[30] Y. Shen, Y. Lv, Dual targeted zeolitic imidazolate framework nanoparticles for treating metastatic breast cancer and inhibiting bone destruction, Colloids Surf. B: Biointerfaces 219 (2022), 112826.

[31] C. Shuai, X. Yuan, Y. Shuai, G. Qian, J. Yao, W. Xu, S. Peng, W. Yang, Nitrogen-doped carbon-ZnO heterojunction derived from ZIF-8: a photocatalytic antibacterial strategy for scaffold, Mater. Today Nano 18 (2022), https://doi.org/10.1016/j.mtnano.2022.100210.

[32] Y. Zhao, H. Wang, X. Zou, D. Wang, Y. Fan, X. Zhao, M. Li, L. Yang, C. Liang, Antibacterial vancomycin@ZIF-8 loaded PVA nanofiber membrane for infected bone repair, Int. J. Mol. Sci. 23 (10) (2022), https://doi.org/10.3390/ijms23105629.

[33] X. Cheng, Z. Zhu, Y. Liu, Y. Xue, X. Gao, J. Wang, X. Pei, Q. Wan, Zeolitic Imidazolate Framework-8 encapsulating Risedronate synergistically enhances osteogenic and Antiresorptive properties for bone regeneration, ACS Biomater Sci. Eng. 6 (4) (2020) 2186–2197.

[34] L. Shi, J. Wu, X. Qiao, Y. Ha, Y. Li, C. Peng, R. Wu, In situ biomimetic mineralization on ZIF-8 for smart drug delivery, ACS Biomater Sci. Eng. 6 (8) (2020) 4595–4603.

[35] H. Feng, Z. Li, W. Xie, Q. Wan, Y. Guo, J. Chen, J. Wang, X. Pei, Delivery of therapeutic miRNAs using nanoscale zeolitic imidazolate framework for accelerating vascularized bone regeneration, Chem. Eng. J. 430 (2022), 132867.

[36] Q. Xu, Z. Chen, Y. Zhang, X. Hu, F. Chen, L. Zhang, N. Zhong, J. Zhang, Y. Wang, Mussel-inspired bioactive 3D-printable poly(styrene-butadiene-styrene) and the in vitro assessment of its potential as cranioplasty implants, J. Mater. Chem. B 10 (19) (2022) 3747–3758.

[37] H. Pan, X. Miao, J. Deng, C. Pan, X. Cheng, X. Wang, Bimetallic metal-organic framework for mitigating aseptic Osteolysis, ACS Appl. Mater. Interfaces (2023), https://doi.org/10.1021/acsami.2c19449.

[38] Y. Zhu, Q. Zhi, C. Zhang, Y. Gu, S. Liu, S. Qiao, H. Lai, Debridement of contaminated implants using air-polishing coupled with pH-responsive maximin H5-embedded metal-organic frameworks, Front. Bioeng. Biotechnol. 11 (2023), https://doi.org/10.3389/fbioe.2023.1124107.

[39] Y. Jiang, X. Pan, M. Yao, L. Han, X. Zhang, Z. Jia, J. Weng, W. Chen, L. Fang, X. Wang, Y. Zhang, R. Duan, F. Ren, K. Wang, X. Chen, X. Lu, Bioinspired adhesive and tumor microenvironment responsive nanoMOFs assembled 3D-printed scaffold for anti-tumor therapy and bone regeneration, Nano Today 39 (2021), 101182.

[40] M. Sun, Y. Liu, K. Jiao, W. Jia, K. Jiang, Z. Cheng, G. Liu, Y. Luo, A periodontal tissue regeneration strategy via biphasic release of zeolitic imidazolate framework-8 and FK506 using a uniaxial electrospun Janus nanofiber, J. Mater. Chem. B 10 (5) (2022) 765–778.

[41] J. Chen, X. Zhang, C. Huang, H. Cai, S. Hu, Q. Wan, X. Pei, J. Wang, Osteogenic activity and antibacterial effect of porous titanium modified with metal-organic framework films, J. Biomed. Mater. Res. A 105 (3) (2017) 834–846.

[42] X. Zhang, J. Chen, X. Pei, J. Wang, Q. Wan, S. Jiang, C. Huang, X. Pei, Enhanced Osseointegration of porous titanium modified with Zeolitic Imidazolate Framework-8, ACS Appl. Mater. Interfaces 9 (30) (2017) 25171–25183.

[43] J. Ran, H. Zeng, J. Cai, P. Jiang, P. Yan, L. Zheng, Y. Bai, X. Shen, B. Shi, H. Tong, Rational design of a stable, effective, and sustained dexamethasone delivery platform on a titanium implant: An innovative application of metal organic frameworks in bone implants, Chem. Eng. J. 333 (2018) 20–33.

[44] X. Zhang, J. Wang, J. Wu, X. Jiang, X. Pei, J. Chen, Q. Wan, C. Huang, Dimethyloxalylglycine improves angiogenesis of ZIF-8-coated implant, J. Biomater. Appl. 34 (3) (2019) 396–407.

[45] F. Ejeian, A. Razmjou, M.H. Nasr-Esfahani, M. Mohammad, F. Karamali, M. Ebrahimi Warkiani, M. Asadnia, V. Chen, ZIF-8 modified polypropylene membrane: a biomimetic cell culture platform with a view to the improvement of guided bone regeneration, Int. J. Nanomedicine 15 (2020) 10029–10043.

[46] Y. Liu, Z. Zhu, X. Pei, X. Zhang, X. Cheng, S. Hu, X. Gao, J. Wang, J. Chen, Q. Wan, ZIF-8-modified multifunctional bone-adhesive hydrogels promoting angiogenesis and osteogenesis for bone regeneration, ACS Appl. Mater. Interfaces 12 (33) (2020) 36978–36995.

[47] B. Tao, W. Zhao, C. Lin, Z. Yuan, Y. He, L. Lu, M. Chen, Y. Ding, Y. Yang, Z. Xia, K. Cai, Surface modification of titanium implants by ZIF-8@Levo/LBL coating for inhibition of bacterial-associated infection and enhancement of in vivo osseointegration, Chem. Eng. J. 390 (2020), 124621.

[48] L. Zhong, J. Chen, Z. Ma, H. Feng, S. Chen, H. Cai, Y. Xue, X. Pei, J. Wang, Q. Wan, 3D printing of metal-organic framework incorporated porous scaffolds to promote osteogenic differentiation and bone regeneration, Nanoscale 12 (48) (2020) 24437–24449.

[49] Y. Chen, Q. Yang, D. Ma, L. Peng, Y. Mao, X. Zhou, Y. Deng, W. Yang, Metal-organic frameworks/polydopamine coating endows polyetheretherketone with disinfection and osteogenicity, Int. J. Polym. Mater. Polym. Biomater. 71 (10) (2021) 783–794.

[50] M.A. Fardjahromi, F. Ejeian, A. Razmjou, G. Vesey, S.C. Mukhopadhyay, A. Derakhshan, M.E. Warkiani, Enhancing osteoregenerative potential of biphasic calcium phosphates by using bioinspired ZIF8 coating, Mater. Sci. Eng. C Mater. Biol. Appl. 123 (2021), 111972.

[51] X. Gao, Y. Xue, Z. Zhu, J. Chen, Y. Liu, X. Cheng, X. Zhang, J. Wang, X. Pei, Q. Wan, Nanoscale Zeolitic Imidazolate Framework-8 activator of canonical MAPK signaling for bone repair, ACS Appl. Mater. Interfaces 13 (1) (2021) 97–111.

[52] W. Teng, Z. Zhang, Y. Wang, Y. Ye, E. Yinwang, A. Liu, X. Zhou, J. Xu, C. Zhou, H. Sun, F. Wang, L. Zhang, C. Cheng, P. Lin, Y. Wu, Z. Gou, X. Yu, Z. Ye, Iodine immobilized metal-organic framework for NIR-triggered antibacterial therapy on orthopedic implants, Small 17 (35) (2021), e2102315.

[53] Ö. Toprak, B. Topuz, Y.A. Monsef, Ç. Oto, K. Orhan, A. Karakeçili, BMP-6 carrying metal organic framework-embedded in bioresorbable electrospun fibers for enhanced bone regeneration, Mater. Sci. Eng. C Mater. Biol. Appl. 120 (2021), 111738.

[54] Y. Xue, Z. Zhu, X. Zhang, J. Chen, X. Yang, X. Gao, S. Zhang, F. Luo, J. Wang, W. Zhao, C. Huang, X. Pei, Q. Wan, Accelerated bone regeneration by MOF modified multifunctional membranes through enhancement of osteogenic and Angiogenic performance, Adv. Healthc. Mater. 10 (6) (2021), e2001369.

[55] M.A. Al-Baadani, L. Xu, K.H.R. Yie, A. Sun, X. Gao, K. Cai, B.A. Al-Shaaobi, A. M. Al-Bishari, L. Cai, X. Shen, J. Liu, P. Ma, In situ preparation of alendronate-loaded ZIF-8 nanoparticles on electrospun nanofibers for accelerating early osteogenesis in osteoporosis, Mater. Des. 217 (2022), https://doi.org/10.1016/j.matdes.2022.110596.

[56] Y. Deng, J. Shi, Y.K. Chan, D. Bai, R. Shu, X. Shi, Y. Li, L. Li, X. Yang, W. Yang, Heterostructured metal-organic frameworks/Polydopamine coating endows Polyetheretherketone implants with multimodal Osteogenicity and Photoswitchable disinfection, Adv. Healthc. Mater. 11 (14) (2022), e2200641.

[57] Y. Ge, K. Wang, J. Liu, Y. Tian, H. Li, H. Wang, Z. Lin, M. Qiu, B. Tang, A ZIF-8-based multifunctional intelligent drug release system for chronic osteomyelitis, Colloids Surf. B: Biointerfaces 212 (2022), https://doi.org/10.1016/j.colsurfb.2022.112354.

[58] N. Liang, N. Ren, Z. Feng, Z. Sun, M. Dong, W. Wang, F. Liu, C. Sun, W. Zhou, Z. Xing, J. Wang, C. Liu, H. Liu, Biomimetic metal-organic frameworks as targeted vehicles to enhance osteogenesis, Adv. Healthc. Mater. 11 (12) (2022), e2102821.

[59] L. Ling, S. Cai, Y. Zuo, M. Tian, T. Meng, H. Tian, X. Bao, G. Xu, Copper-doped zeolitic imidazolate frameworks-8/hydroxyapatite composite coating endows magnesium alloy with excellent corrosion resistance, antibacterial ability and biocompatibility, Colloids Surf. B: Biointerfaces 219 (2022), https://doi.org/10.1016/j.colsurfb.2022.112810.

[60] R. Liu, Y. Pang, T. Xiao, S. Zhang, Y. Liu, Y. Min, Multifunctional PCL composite nanofibers reinforced with lignin and ZIF-8 for the treatment of bone defects, Int. J. Biol. Macromol. 218 (2022) 1–8.

[61] Y. Liu, T. Li, M. Sun, Z. Cheng, W. Jia, K. Jiao, S. Wang, K. Jiang, Y. Yang, Z. Dai, L. Liu, G. Liu, Y. Luo, ZIF-8 modified multifunctional injectable photopolymerizable GelMA hydrogel for the treatment of periodontitis, Acta Biomater. 146 (2022) 37–48.

[62] T. Ni, Y. Zhu, L. Hao, Y. Chen, T. Cheng, Preparation of photothermal-sensitive PDGF@ZIF-8-PDA@COL/PLGA-TCP composite scaffolds for bone defect repair, Mater. Des. 217 (2022), https://doi.org/10.1016/j.matdes.2022.110643.

[63] Y. Pan, K. Huang, Y. Li, Y. Liu, H. Yu, Z. Lv, R. Zou, Q. Yao, Mesoporous porphyrinic metal-organic framework nanoparticles/3D nanofibrous scaffold as a versatile platform for bone tumor therapy, Mater. Today Chem. 24 (2022), https://doi.org/10.1016/j.mtchem.2022.100829.

[64] M. Qiao, Z. Xu, X. Pei, Y. Liu, J. Wang, J. Chen, Z. Zhu, Q. Wan, Nano SIM@ZIF-8 modified injectable high-intensity biohydrogel with bidirectional regulation of osteogenesis and anti-adipogenesis for bone repair, Chem. Eng. J. 434 (2022), 134583.

[65] N. Ren, N. Liang, M. Dong, Z. Feng, L. Meng, C. Sun, A. Wang, X. Yu, W. Wang, J. Xie, C. Liu, H. Liu, Stem cell membrane-encapsulated Zeolitic Imidazolate Framework-8: a targeted Nano-platform for osteogenic differentiation, Small 18 (26) (2022), e2202485.

[66] W. Shi, L. Bian, Y. Wu, Z. Wang, Y. Dai, Y. Zhou, P. Meng, Q. Wang, Z. Zhang, X. Zhao, P. Zhao, X. Lu, Enhanced bone regeneration using a ZIF-8-loaded fibrin composite scaffold, Macromol. Biosci. 22 (3) (2022), e2100416.

[67] L. Wang, F. Dai, Y. Tang, Z. Zhang, Zeolitic Imidazolate Framework-8 with encapsulated Naringin synergistically improves antibacterial and osteogenic properties of Ti implants for Osseointegration, ACS Biomater. Sci. Eng. 8 (9) (2022) 3797–3809.

[68] X. Wang, X. Qiu, J. Pei, D. Zhao, Y. Yan, Fabrication of magnesium phosphate bone cement with enhanced osteogenic properties by employing zeolitic imidazolate framework-8, J. Mater. Res. 37 (17) (2022) 2761–2774.

[69] X. Zhang, J.Y. Chen, X. Pei, Y.H. Li, H. Feng, Z.H. He, W.J. Xie, X.B. Pei, Z. Zhu, Q. B. Wan, J. Wang, One-pot facile encapsulation of dimethyloxallyl glycine by nanoscale zeolitic imidazolate frameworks-8 for enhancing vascularized bone regeneration, Adv Healthc Mater. 12 (4) (2022), e2202317.

[70] Z.Y. Chen, R.B. Zhou, R.D. Wang, S.L. Su, F. Zhou, Dual-crosslinked network of polyacrylamide-carboxymethylcellulose hydrogel promotes osteogenic differentiation in vitro, Int. J. Biol. Macromol. 234 (2023), 123788.

[71] S. Hu, S. Wang, Q. He, D. Li, L. Xin, C. Xu, X. Zhu, L. Mei, R.D. Cannon, P. Ji, H. Tang, T. Chen, A mechanically reinforced super bone glue makes a leap in hard tissue strong adhesion and augmented bone regeneration, Adv Sci (Weinh) 10 (11) (2023), e2206450.

[72] A. Lao, J. Wu, D. Li, A. Shen, Y. Li, Y. Zhuang, K. Lin, J. Wu, J. Liu, Functionalized metal-organic framework-modified hydrogel that breaks the vicious cycle of inflammation and ROS for repairing of diabetic bone defects, Small (2023), https://doi.org/10.1002/smll.202206919.

[73] W. Li, A. Tian, T. Li, Y. Zhao, M. Chen, Ag/ZIF-8/mg-Al LDH composite coating on MAO pretreated mg alloy as a multi-ion-release platform to improve corrosion resistance, osteogenic activity, and photothermal antibacterial properties, Surf. Coat. Technol. 464 (2023), https://doi.org/10.1016/j.surfcoat.2023.129555.

[74] Y. Li, J. Zhu, X. Zhang, Y. Li, S. Zhang, L. Yang, R. Li, Q. Wan, X. Pei, J. Chen, J. Wang, Drug-delivery Nanoplatform with synergistic regulation of angiogenesis-osteogenesis coupling for promoting vascularized bone regeneration, ACS Appl. Mater. Interfaces 15 (14) (2023) 17543–17561.

[75] Z. Shu, C. Zhang, L. Yan, H. Lei, C. Peng, S. Liu, L. Fan, Y. Chu, Antibacterial and osteoconductive polycaprolactone/polylactic acid/nano-hydroxyapatite/cu@ZIF-8 GBR membrane with asymmetric porous structure, Int. J. Biol. Macromol. 224 (2023) 1040–1051.

[76] Y. Si, H. Liu, M. Li, X. Jiang, H. Yu, D. Sun, An efficient metal–organic framework-based drug delivery platform for synergistic antibacterial activity and osteogenesis, J. Colloid Interface Sci. 640 (2023) 521–539.

[77] Z. Xu, Y. Zhang, D. Lu, G. Zhang, Y. Li, Z. Lu, F. Wang, G. Wang, Antisenescence ZIF-8/resveratrol Nanoformulation with potential for enhancement of bone fracture healing in the elderly, ACS Biomater. Sci. Eng. 9 (5) (2023) 2636–2646.

[78] H. Zhang, D. Liu, Y. Yao, B. Zhang, Y.S. Lin, Stability of ZIF-8 membranes and crystalline powders in water at room temperature, J. Membr. Sci. 485 (2015) 103–111.

[79] H. Zheng, Y. Zhang, L. Liu, W. Wan, P. Guo, A.M. Nystrom, X. Zou, One-pot synthesis of metal-organic frameworks with encapsulated target molecules and their applications for controlled drug delivery, J. Am. Chem. Soc. 138 (3) (2016) 962–968.

[80] X. Qian, Q. Ren, X. Wu, J. Sun, H. Wu, J. Lei, Enhanced water stability in Zn-doped Zeolitic Imidazolate Framework-67 (ZIF-67) for CO2 capture applications, ChemistrySelect 3 (2) (2018) 657–661.

[81] M.A. Luzuriaga, C.E. Benjamin, M.W. Gaertner, H. Lee, F.C. Herbert, S. Mallick, J. J. Gassensmith, ZIF-8 degrades in cell media, serum, and some—but not all—common laboratory buffers, Supramol. Chem. 31 (8) (2019) 485–490.

[82] M.D.J. Velásquez-Hernández, R. Ricco, F. Carraro, F.T. Limpoco, M. Linares-Moreau, E. Leitner, H. Wiltsche, J. Rattenberger, H. Schröttner, P. Frühwirt, E. M. Stadler, G. Gescheidt, H. Amenitsch, C.J. Doonan, P. Falcaro, Degradation of

ZIF-8 in phosphate buffered saline media, CrystEngComm 21 (31) (2019) 4538–4544.

[83] M. Taheri, D. Ashok, T. Sen, T.G. Enge, N.K. Verma, A. Tricoli, A. Lowe, D. R. Nisbet, T. Tsuzuki, Stability of ZIF-8 nanopowders in bacterial culture media and its implication for antibacterial properties, Chem. Eng. J. 413 (2021).

[84] A.S. Spitsyna, A.S. Poryvaev, N.E. Sannikova, A.A. Yazikova, I.A. Kirilyuk, S. A. Dobrynin, O.A. Chinak, M.V. Fedin, O.A. Krumkacheva, Stability of ZIF-8 nanoparticles in Most common cell culture media, Molecules 27 (10) (2022).

[85] M. Abendrot, L. Chęcińska, J. Kusz, K. Lisowska, K. Zawadzka, A. Felczak, U. Kalinowska-Lis, Zinc(II) complexes with amino acids for potential use in dermatology: synthesis, crystal structures, and antibacterial activity, Molecules 25 (4) (2020).

[86] N. Pace, E. Weerapana, Zinc-binding cysteines: diverse functions and structural motifs, Biomolecules 4 (2) (2014) 419–434.

[87] W. Cai, J. Wang, C. Chu, W. Chen, C. Wu, G. Liu, Metal-organic framework-based stimuli-responsive Systems for Drug Delivery, Adv Sci (Weinh) 6 (1) (2019) 1801526.

[88] F. Peng, D. Wang, D. Zhang, B. Yan, H. Cao, Y. Qiao, X. Liu, PEO/Mg-Zn-Al LDH composite coating on mg alloy as a Zn/mg ion-release platform with multifunctions: enhanced corrosion resistance, osteogenic, and antibacterial activities, ACS Biomater Sci Eng 4 (12) (2018) 4112–4121.

[89] C. Wiegand, U.C. Hipler, Methods for the measurement of cell and tissue compatibility including tissue regeneration processes, GMS Krankenhhyg Interdiszip 3 (1) (2008), Doc12.

[90] D.F. Williams, On the mechanisms of biocompatibility, Biomaterials 29 (20) (2008) 2941–2953.

[91] S.X. Li, K.K. Wang, Y.J. Shi, Y.N. Cui, B.L. Chen, B. He, W.B. Dai, H. Zhang, X. Q. Wang, C.L. Zhong, H.N. Wu, Q.Y. Yang, Q. Zhang, Novel biological functions of ZIF-NP as a delivery vehicle: high pulmonary accumulation, favorable biocompatibility, and improved therapeutic outcome, Adv. Funct. Mater. 26 (16) (2016) 2715–2727.

[92] J.D. Johnson, D. Reichelderfer, A. Zutshi, S. Graves, D. Walters, C. Smith, Toxicokinetics of 2-methylimidazole in male and female F344 rats, J. Toxicol. Environ. Health A 65 (12) (2002) 869–879.

[93] I.W.G.o.t.E.o.C.R.t. Humans, Some chemicals present in industrial and consumer products, food and drinking-water, IARC Monogr. Eval. Carcinog. Risks Hum. 101 (2013) 9–549.

[94] T.A. Link, G. von Jagow, Zinc ions inhibit the QP center of bovine heart mitochondrial bc1 complex by blocking a protonatable group, J. Biol. Chem. 270 (42) (1995) 25001–25006.

[95] A. Clausen, T. McClanahan, S.G. Ji, J.H. Weiss, Mechanisms of rapid reactive oxygen species generation in response to cytosolic Ca2+ or Zn2+ loads in cortical neurons, PLoS One 8 (12) (2013), e83347.

[96] K.E. Dineley, T.V. Votyakova, I.J. Reynolds, Zinc inhibition of cellular energy production: implications for mitochondria and neurodegeneration, J. Neurochem. 85 (3) (2003) 563–570.

[97] L.J. Martin, N.A. Adams, Y. Pan, A. Price, M. Wong, The mitochondrial permeability transition pore regulates nitric oxide-mediated apoptosis of neurons induced by target deprivation, J. Neurosci. 31 (1) (2011) 359–370.

[98] T. Thorn, R. Gniadecki, A.B. Petersen, J. Vicanova, H.C. Wulf, Differences in activation of G2/M checkpoint in keratinocytes after genotoxic stress induced by hydrogen peroxide and ultraviolet a radiation, Free Radic. Res. 35 (4) (2001) 405–416.

[99] M.S. Cooke, M.D. Evans, M. Dizdaroglu, J. Lunec, Oxidative DNA damage: mechanisms, mutation, and disease, FASEB J. 17 (10) (2003) 1195–1214.

[100] K.F. Hua, P.C. Liao, Z. Fang, F.L. Yang, Y.L. Yang, Y.L. Chen, Y.C. Chiu, M.L. Liu, Y. Lam, S.H. Wu, Generation of reactive oxygen species by polyenylpyrroles derivatives causes DNA damage leading to G2/M arrest and apoptosis in human oral squamous cell carcinoma cells, PLoS One 8 (6) (2013), e67603.

[101] M. Hoop, C.F. Walde, R. Riccò, F. Mushtaq, A. Terzopoulou, X.-Z. Chen, A. J. deMello, C.J. Doonan, P. Falcaro, B.J. Nelson, J. Puigmartí-Luis, S. Pané, Biocompatibility characteristics of the metal organic framework ZIF-8 for therapeutical applications, Appl. Mater. Today 11 (2018) 13–21.

[102] S. Kumari, T.S. Howlett, R.N. Ehrman, S. Koirala, O. Trashi, I. Trashi, Y. H. Wijesundara, J.J. Gassensmith, In vivo biocompatibility of ZIF-8 for slow release via intranasal administration, Chem. Sci. 14 (21) (2023) 5774–5782.

[103] G. Jin, H. Cao, Y. Qiao, F. Meng, H. Zhu, X. Liu, Osteogenic activity and antibacterial effect of zinc ion implanted titanium, Colloids Surf. B: Biointerfaces 117 (2014) 158–165.

[104] S. Pina, S.I. Vieira, P. Rego, P.M. Torres, O.A. da Cruz e Silva, E.F. da Cruz e Silva, J.M. Ferreira, Biological responses of brushite-forming Zn- and ZnSr- substituted beta-tricalcium phosphate bone cements, Eur. Cell. Mater. 20 (2010) 162–177.

[105] S. Kanno, C.D. Anuradha, S. Hirano, Chemotactic responses of osteoblastic MC3T3-E1 cells toward zinc chloride, Biol. Trace Elem. Res. 83 (1) (2001) 49–55.

[106] H. Hu, W. Zhang, Y. Qiao, X. Jiang, X. Liu, C. Ding, Antibacterial activity and increased bone marrow stem cell functions of Zn-incorporated TiO2 coatings on titanium, Acta Biomater. 8 (2) (2012) 904–915.

[107] X. Shen, Y. Hu, G. Xu, W. Chen, K. Xu, Q. Ran, P. Ma, Y. Zhang, J. Li, K. Cai, Regulation of the biological functions of osteoblasts and bone formation by Zn-incorporated coating on microrough titanium, ACS Appl. Mater. Interfaces 6 (18) (2014) 16426–16440.

[108] I.S. Kwun, Y.E. Cho, R.A. Lomeda, H.I. Shin, J.Y. Choi, Y.H. Kang, J.H. Beattie, Zinc deficiency suppresses matrix mineralization and retards osteogenesis transiently with catch-up possibly through Runx 2 modulation, Bone 46 (3) (2010) 732–741.

[109] N.J. Lakhkar, I.H. Lee, H.W. Kim, V. Salih, I.B. Wall, J.C. Knowles, Bone formation controlled by biologically relevant inorganic ions: role and controlled delivery from phosphate-based glasses, Adv. Drug Deliv. Rev. 65 (4) (2013) 405–420.

[110] H. Wang, S. Zhao, W. Xiao, J. Cui, W. Huang, M.N. Rahaman, C. Zhang, D. Wang, Three-dimensional zinc incorporated borosilicate bioactive glass scaffolds for rodent critical-sized calvarial defects repair and regeneration, Colloids Surf. B: Biointerfaces 130 (2015) 149–156.

[111] J. Chou, M. Komuro, J. Hao, S. Kuroda, Y. Hattori, B. Ben-Nissan, B. Milthorpe, M. Otsuka, Bioresorbable zinc hydroxyapatite guided bone regeneration membrane for bone regeneration, Clin. Oral Implants Res. 27 (3) (2016) 354–360.

[112] D. Zhu, Y. Su, M.L. Young, J. Ma, Y. Zheng, L. Tang, Biological responses and mechanisms of human bone marrow mesenchymal stem cells to Zn and mg biomaterials, ACS Appl. Mater. Interfaces 9 (33) (2017) 27453–27461.

[113] K.H. Park, Y. Choi, D.S. Yoon, K.M. Lee, D. Kim, J.W. Lee, Zinc promotes osteoblast differentiation in human mesenchymal stem cells via activation of the cAMP-PKA-CREB signaling pathway, Stem Cells Dev. 27 (16) (2018) 1125–1135.

[114] Y. Qiao, W. Zhang, P. Tian, F. Meng, H. Zhu, X. Jiang, X. Liu, P.K. Chu, Stimulation of bone growth following zinc incorporation into biomaterials, Biomaterials 35 (25) (2014) 6882–6897.

[115] J. An, H. Yang, Q. Zhang, C. Liu, J. Zhao, L. Zhang, B. Chen, Natural products for treatment of osteoporosis: the effects and mechanisms on promoting osteoblast-mediated bone formation, Life Sci. 147 (2016) 46–58.

[116] L. Liu, Q. Luo, J. Sun, Y. Ju, Y. Morita, G. Song, Chromatin organization regulated by EZH2-mediated H3K27me3 is required for OPN-induced migration of bone marrow-derived mesenchymal stem cells, Int. J. Biochem. Cell Biol. 96 (2018) 29–39.

[117] M.L. Cancela, V. Laize, N. Conceicao, Matrix Gla protein and osteocalcin: from gene duplication to neofunctionalization, Arch. Biochem. Biophys. 561 (2014) 56–63.

[118] X. Yuan, R.J. Smith Jr., H. Guan, C.N. Ionita, P. Khobragade, R. Dziak, Z. Liu, M. Pang, C. Wang, G. Guan, S. Andreadis, S. Yang, Hybrid biomaterial with conjugated growth factors and mesenchymal stem cells for ectopic bone formation, Tissue Eng. Part A 22 (13–14) (2016) 928–939.

[119] G.A. Fielding, W. Smoot, S. Bose, Effects of SiO2, SrO, MgO, and ZnO dopants in tricalcium phosphates on osteoblastic Runx2 expression, J. Biomed. Mater. Res. A 102 (7) (2014) 2417–2426.

[120] A. Nishiguchi, T. Taguchi, Osteoclast-responsive, injectable bone of Bisphosphonated-Nanocellulose that regulates osteoclast/osteoblast activity for bone regeneration, Biomacromolecules 20 (3) (2019) 1385–1393.

[121] X. Liu, Y. Ma, M. Chen, J. Ji, Y. Zhu, Q. Zhu, M. Guo, P. Zhang, Ba/mg co-doped hydroxyapatite/PLGA composites enhance X-ray imaging and bone defect regeneration, J. Mater. Chem. B 9 (33) (2021) 6691–6702.

[122] J. Tan, D. Wang, H. Cao, Y. Qiao, H. Zhu, X. Liu, Effect of local alkaline microenvironment on the behaviors of Bacteria & osteogenic cells, ACS Appl. Mater. Interfaces 10 (49) (2018) 42018–42029.

[123] L. Pontiroli, M. Dadkhah, G. Novajra, I. Tcacencu, S. Fiorilli, C. Vitale-Brovarone, An aerosol-spray-assisted approach to produce mesoporous bioactive glass microspheres under mild acidic aqueous conditions, Mater. Lett. 190 (2017) 111–114.

[124] J.P. O'Connor, D. Kanjilal, M. Teitelbaum, S.S. Lin, J.A. Cottrell, Zinc as a therapeutic agent in bone regeneration, Materials (Basel) 13 (10) (2020), https://doi.org/10.3390/ma13102211.

[125] E.W. Zhang, Y.B. Wang, K.G. Shuai, F. Gao, Y.J. Bai, Y. Cheng, X.L. Xiong, Y. F. Zheng, S.C. Wei, In vitro and in vivo evaluation of SLA titanium surfaces with further alkali or hydrogen peroxide and heat treatment, Biomed. Mater. 6 (2) (2011), 025001.

[126] K. Chen, L. Zhao, J. Sun, X. Gu, C. Huang, H. Su, Y. Fan, Utilizing biodegradable alloys as guided bone regeneration (GBR) membrane: feasibility and challenges, Sci. China Mater. 65 (10) (2022) 2627–2646.

[127] R. Wang, J. Ozsvar, B. Aghaei-Ghareh-Bolagh, M.A. Hiob, S.M. Mithieux, A. S. Weiss, Freestanding hierarchical vascular structures engineered from ice, Biomaterials 192 (2019) 334–345.

[128] A. Aurora, N. Wrice, T.J. Walters, R.J. Christy, S. Natesan, A PEGylated platelet free plasma hydrogel based composite scaffold enables stable vascularization and targeted cell delivery for volumetric muscle loss, Acta Biomater. 65 (2018) 150–162.

[129] D.P. Bhattarai, M.H. Kim, H. Park, W.H. Park, B.S. Kim, C.S. Kim, Coaxially fabricated polylactic acid electrospun nanofibrous scaffold for sequential release of tauroursodeoxycholic acid and bone morphogenic protein2 to stimulate angiogenesis and bone regeneration, Chem. Eng. J. 389 (2020), 123470.

[130] Y. Hanai, H. Tokuda, E. Yasuda, T. Noda, T. Ohta, S. Takai, O. Kozawa, Up-regulation by zinc of FGF-2-induced VEGF release through enhancing p44/p42 MAP kinase activation in osteoblasts, Life Sci. 80 (3) (2006) 230–234.

[131] P. Carmeliet, Angiogenesis in life, disease and medicine, Nature 438 (7070) (2005) 932–936.

[132] C. Peach, V. Mignone, M. Arruda, D. Alcobia, S. Hill, L. Kilpatrick, J. Woolard, Molecular pharmacology of VEGF-A isoforms: binding and Signalling at VEGFR2, Int. J. Mol. Sci. 19 (4) (2018).

[133] N. Ferrara, A.P. Adamis, Ten years of anti-vascular endothelial growth factor therapy, Nat. Rev. Drug Discov. 15 (6) (2016) 385–403.

[134] Y. Li, T. Ma, X. Zhu, M. Zhang, L. Zhao, P. Wang, J. Liang, Zinc improves neurological recovery by promoting angiogenesis via the astrocyte-mediated HIF-1α/VEGF signaling pathway in experimental stroke, CNS Neurosci. Ther. 28 (11) (2022) 1790–1799.

[135] K. Holmqvist, M.J. Cross, C. Rolny, R. Hägerkvist, N. Rahimi, T. Matsumoto, L. Claesson-Welsh, M. Welsh, The adaptor protein shb binds to tyrosine 1175 in

vascular endothelial growth factor (VEGF) receptor-2 and regulates VEGF-dependent cellular migration, J. Biol. Chem. 279 (21) (2004) 22267–22275.

[136] X.L. Chen, J.-O. Nam, C. Jean, C. Lawson, C.T. Walsh, E. Goka, S.-T. Lim, A. Tomar, I. Tancioni, S. Uryu, J.-L. Guan, L.M. Acevedo, S.M. Weis, D.A. Cheresh, D.D. Schlaepfer, VEGF-induced vascular permeability is mediated by FAK, Dev. Cell 22 (1) (2012) 146–157.

[137] M.E. McMullen, P.W. Bryant, C.C. Glembotski, P.A. Vincent, K.M. Pumiglia, Activation of p38 has opposing effects on the proliferation and migration of endothelial cells, J. Biol. Chem. 280 (22) (2005) 20995–21003.

[138] M.Y. Lee, A.K. Luciano, E. Ackah, J. Rodriguez-Vita, T.A. Bancroft, A. Eichmann, M. Simons, T.R. Kyriakides, M. Morales-Ruiz, W.C. Sessa, Endothelial Akt1 mediates angiogenesis by phosphorylating multiple angiogenic substrates, Proc. Natl. Acad. Sci. U. S. A. 111 (35) (2014) 12865–12870.

[139] Z. Kang, H. Zhu, W. Jiang, S. Zhang, Protocatechuic acid induces angiogenesis through PI3K-Akt-eNOS-VEGF signalling pathway, Basic Clin. Pharmacol. Toxicol. 113 (4) (2013) 221–227.

[140] T. Takahashi, H. Ueno, M. Shibuya, VEGF activates protein kinase C-dependent, but Ras-independent Raf-MEK-MAP kinase pathway for DNA synthesis in primary endothelial cells, Oncogene 18 (13) (1999) 2221–2230.

[141] T. Takahashi, S. Yamaguchi, K. Chida, M. Shibuya, A single autophosphorylation site on KDR/Flk-1 is essential for VEGF-A-dependent activation of PLC-gamma and DNA synthesis in vascular endothelial cells, EMBO J. 20 (11) (2001) 2768–2778.

[142] R. Abu-Ghazaleh, J. Kabir, H. Jia, M. Lobo, I. Zachary, Src mediates stimulation by vascular endothelial growth factor of the phosphorylation of focal adhesion kinase at tyrosine 861, and migration and anti-apoptosis in endothelial cells, Biochem. J. 360 (Pt 1) (2001) 255–264.

[143] H.P. Gerber, A. McMurtrey, J. Kowalski, M. Yan, B.A. Keyt, V. Dixit, N. Ferrara, Vascular endothelial growth factor regulates endothelial cell survival through the phosphatidylinositol 3′-kinase/Akt signal transduction pathway. Requirement for Flk-1/KDR activation, J. Biol. Chem. 273 (46) (1998) 30336–30343.

[144] Z. Chen, J. Duan, Y. Diao, Y. Chen, X. Liang, H. Li, Y. Miao, Q. Gao, L. Gui, X. Wang, J. Yang, Y. Li, ROS-responsive capsules engineered from EGCG-zinc networks improve therapeutic angiogenesis in mouse limb ischemia, Bioactive Mater. 6 (1) (2021) 1–11.

[145] D. Zhu, Y. Su, Y. Zheng, B. Fu, L. Tang, Y.-X. Qin, Zinc regulates vascular endothelial cell activity through zinc-sensing receptor ZnR/GPR39, Am. J. Phys. Cell Phys. 314 (4) (2018) C404–C414.